Sine Sweep Load Versus Impact Excitations and their Influence on the Identification of Damping in a Bubbly Oil Squeeze Film Damper

by

Luis E. Rodriguez
Dr. Sergio E. Diaz
Dr. Luis San Andrés

May 2000

TRC-SFD-3-00

EXECUTIVE SUMMARY

Squeeze Film Dampers (*SFD*) are widely used in aircraft gas turbines to suppress excessive vibration and rotordynamic instabilities. However, air ingestion into the oil film due to large amplitudes of vibration is a pervasive phenomenon that considerably affects their performance, making their analysis and design more complicated. Detailed experimentation is required to advance the state of the art in understanding this phenomenon. This study presents the identification of dynamic force coefficients from a small rotor supported on a *SFD*, using the Instrumental Variable Filter method. A controlled mixture of air and oil is fed into the bearing to simulate increasing levels of severity of air entrainment. The objective is to experimentally assess the influence of the excitation function on the estimated system parameters. Thus, the rotor-bearing system is excited with a sine sweep force and the identified force coefficients are compared with those found when impact excitations are applied to the system. The identified stiffness and inertia coefficients show no influence of the excitation type and their estimates are always close to the static measurements. Yet, the damping coefficients are extremely sensitive to the type of force excitation. For impact tests, damping coefficients increase up to 50 percent of air volume content in the mixture. For the sine sweep load excitation, the direct damping coefficients remain nearly constant, except for the no lubricant (dry) condition. The larger and sustained amplitudes of periodic journal motion induced in the sweep sine tests expel the air content from the mixture, thus leaving a pure lubricant film which renders invariant damping coefficients significantly different than those obtained for impact excitations where the journal motions are of small amplitude and short duration. The experimental results, and comparisons with others derived from circular centered motions, demonstrate that *SFDs* operating with bubbly mixtures generate a forced performance that depends greatly on the type of excitation induced.

TABLE OF CONTENTS

LIST OF FIGURES AND TABLES

NOMENCLATURE

c	SFD clearance (0.29 mm)
$C_{SFD,Disk}$	Equivalent damping coefficient at SFD (or Disk) location [N.s/m]
C_{ij}	System damping coefficients [N.s/m]; i,j=x,y
D	SFD diameter (50.8 mm)
$f_{x,y}$	External forces applied to rotor in x and y directions [N]
F	*FFT* of force applied to the rotor [N]
F_{ij}	System flexibility coefficients [m/N];i,j=x,y
I_o	Rotor inertia relative to pivot [kg m^2]
$K_{SFD,Disk}$	Equivalent stiffness coefficient at SFD (or Disk) location [N/m]
K_{ij}	System stiffness coefficients [N/m]; i,j=x,y
L	SFD length (25. 4 mm)
$L_{SFD,Disk}$	Distance between pivot and SFD journal (or Disk) [m]
$M_{SFD,Disk,}$	Equivalent system inertia at SFD (or Disk) location [kg]
M_{ij}	Equivalent inertia coefficients [kg]; i,j=x,y
P_0, P, δP	Ambient pressure, pressure at bearing inlet port and uncertainty [Pa]
Q_{oil}, δQ_{oil}	Measured oil volumetric flow and uncertainty [LPM]
Q_{air}, δQ_{air}	Measured air mass flow and uncertainty in Standard liters per minute [SLPM]
r_{ij}	Correlation Factors for the flexibility matrix of the system; i,j=x,y
T_0	Ambient temperature [K]
T, δT	Temperature at bearing inlet port and uncertainty [K]
t	Time [s]
x,y	Horizontal and vertical displacements of shaft centerline [m]
X, Y	*FFT* of horizontal and vertical displacements of shaft centerline [m]
λ	Air volume fraction in mixture [-]
ω	Frequency [rad/s]
θ	Angular displacement of rotor [rad]
μ	Lubricant viscosity [Pa.s]

INTRODUCTION

Squeeze film damper (*SFDs*) are used in high performance turbomachinery to attenuate rotor bearing synchronous vibration response and to eliminate subsynchronous instabilities not adequately handled by conventional bearings [1][1]. A *SFD*, as shown in Figure 1, consists of a lubricant film bounded by a whirling and non-rotating journal and a stationary bearing. In most applications, the outer race of a rolling element bearing serves as the damper journal [2] and it is restrained from spinning by a centering elastic element (squirrel cage) or a dowel pin. In operation, the journal motion squeezes the lubricant within the damper clearance and generates the hydrodynamic pressures (and film forces) able to dissipate the mechanical energy due to rotor vibrations [2, 3].

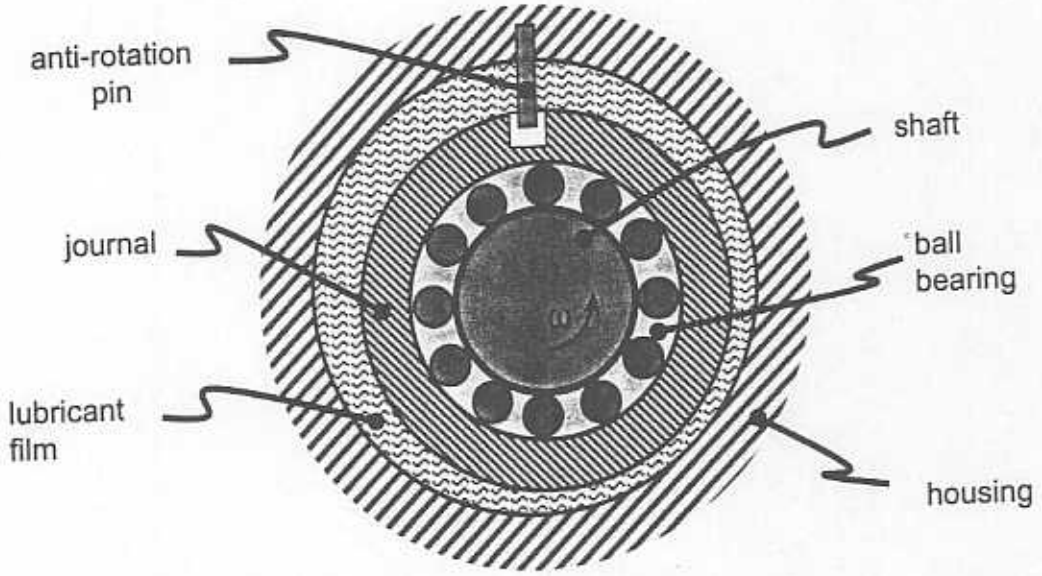

Figure 1. Typical SFD Configuration.

SFD performance is not only determined by factors like geometry (size and clearance) and type of lubricant, but also affected by a number of specific design and operating conditions, including the type of journal motion, flow regime and lubricant cavitation [4]. Several regimes of lubricant cavitation under dynamic operating conditions have been identified [5]. One of them, the air in oil mixture regime occurs at sufficiently high whirl speeds and large journal vibration amplitudes where air is ingested into the lubricant film, becomes entrapped, and

[1] Bracketed numbers denote references listed at the end of the report.

severely reduces the damper force performance [3]. A homogenous mixture model that accounts for air entrainment has been advanced in [6] to predict the damping forces in *SFDs* operating with bubbly mixtures. Extensive research currently focuses on gaining physical understanding on the phenomenon of air entrainment and providing experimental data for validation of physically based models that will later aid in a reliable design procedure [7].

A parameter identification procedure to estimate the mechanical parameters (inertia, stiffness and damping) of a small rotor supported on an open-ended *SFD* follows. The technique used is the Instrumental Variable Filter (*IVF*) method, a frequency domain procedure which is an improved variation of the least squares approximation to the system flexibilities [8,9]. The iterative *IVF* method uses as a first approximation the system flexibilities obtained with the least-squares procedure, and then recalculates the parameters until a given criterion is achieved in terms of a reduction in measurement noise/signal ratio and eliminating bias error [10]. Application of this technique is known to render reliable system coefficients within a specified frequency range.

Diaz and San Andrés [8] performed IVF parameter identification experiments from applied impact loads on the same test rig used in the present investigation. A remarkable result of these tests is that the identified damping coefficients increased as the air volume fraction in the mixture increases to about 50 percent in volume content. This particular behavior was ascribed to the nature of the impact excitations that generates fast transient responses of typically small amplitude and that may have prevented the mixture compressibility from affecting the generation of squeeze film pressures.

The present investigation sets in to study the effect of impact loads and sine sweep forced excitations on the estimated system force coefficients in a rotor mounted on a *SFD* operating with a controlled bubbly mixture. For this purpose, electromagnetic shakers are used to excite the rotor with a sine sweep force, and the results are compared to those obtained with impact load excitations.

Shakers and impactors (i.e. impact hammers or guns) are the most common way to excite a mechanical structure. Although the impact is usually simple to implement, there is a certain difficulty in obtaining consistent results depending on factors like hammer tip, magnitude and duration of the imparted load, etc. Impacts have a typically flat FFT, and thus may excite more modes of vibration than those desirable. Furthermore, the sampling frequency should be fast

enough to capture with fidelity the impact load, and the overall recording time must be long enough to cover the whole transient motion to avoid problems of signal leakage.

In sine sweep type excitations, the load shaker assures the repeatability of the load and measured motions, and the excitation frequency range can be programmed arbitrarily through an analog function generator. Furthermore, the sine sweep function is periodic and leakage problems can be discarded [11]. The sine sweep procedure allows experimentation with an entire set of frequencies at once, thus rendering a more efficient method than using single-frequency harmonic forcing functions within the frequency range of interest. In addition, adequate size shakers can render sustained large amplitudes of vibration during the entire testing time window. This represents a significant difference with the impact excitations that may induce small amplitudes of motion for relatively brief periods of time if the system damping ratio is non negligible.

There are several potential issues to consider when using a shaker system for excitation. The shaker is attached to the structure via a force transducer (load cell), which if rigidly attached adds the shaker mass to that of the structure. On the other hand, the shaker should transmit only one component of force in line with the main axes of the load cell [11]. A common solution uses a long slender beam or stinger to connect the shaker and test structure. In order to vibration isolate the structure from the inertia of the shaker system, a stinger should have a low flexural stiffness and a high (axial) compressive stiffness. A procedure to determine the stingers geometry and the shakers support stiffness was followed to avoid this effect [12].

DESCRIPTION OF TEST RIG

Figure 2 presents a sketch of the test rig and the instrumentation set up for force and displacement measurements. A flexible coupling transmits the torque from the drive DC motor and isolates lateral vibration. The steel shaft length and diameter are equal to 305 mm (12") and 9.5 mm (3/8"), respectively. A combination bronze bushing and O-ring at the drive end and a SFD at the rotor midspan support the shaft. A solid disk weighing 0.811 kg (1.8 lb) is located at the free end of the shaft.

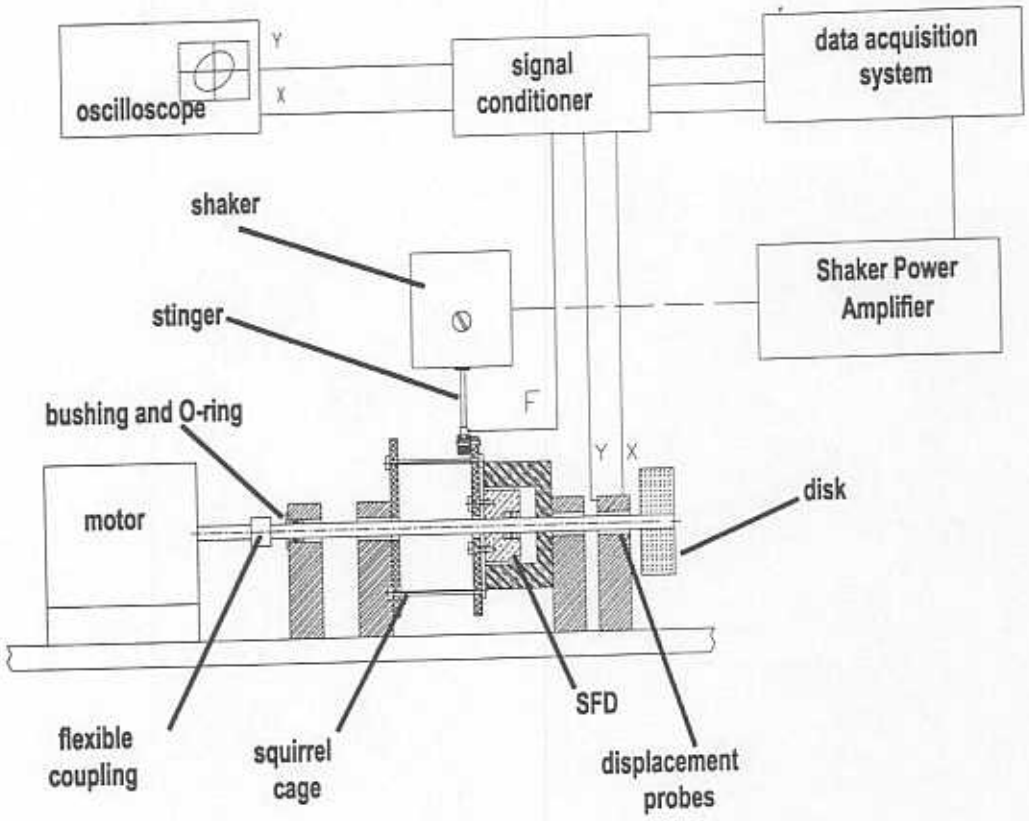

Figure 2. Schematic view of test rig and instrumentation.

The system can be regarded as a rigid body pivoting around the bushing O-ring as shown later. The *SFD* journal and disk centers are at 184 mm (7.23") and 299mm (11.79"), respectively, from the bonze bushing and O-ring location. Two eddy-current displacement sensors installed at L_x=275 mm (10.82") and L_y=260 mm (10.23") measure the shaft horizontal and vertical displacements, respectively.

The squeeze film damper (SFD) consists of a Plexiglas transparent housing and a steel journal of diameter (D) and length (L) equal to 50.8 mm and 25.4 mm respectively. The damper nominal film clearance (c) is 0.29 mm (11.4 mils). The journal connects to the shaft through a pair of rolling element bearings. The centering device of the *SFD* is a squirrel cage consisting of four flexible rods and a plate bolted to the damper journal. All experiments were performed without rotor spinning.

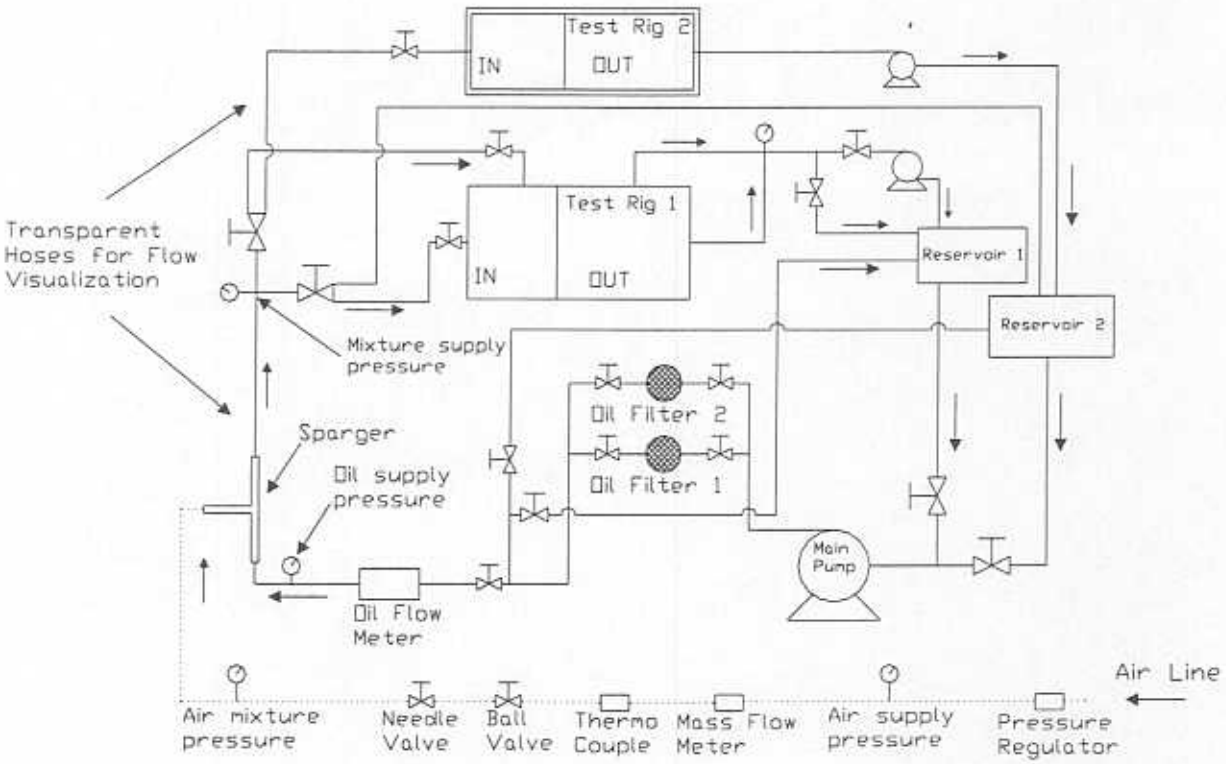

Figure 3. Schematic view of lubricant distribution system.

A modification of the lubricant supply system was performed to share the main pump, mixer and flowmeters with another test rig. Figure 3 shows a simplified sketch of the configuration for the oil feed lines for both test rigs, where the one identified as number two is the apparatus referred in the present study.

The air in oil mixture is generated in the sparger element at the junction of the air and oil lines, as shown in Figure 3. The proportions of air and oil are accurately measured with flowmeters and regulated with valves. The temperature and pressure of the oil and air are measured with thermocouples and pressure gauges, respectively. The instruments uncertainties are 1% of measurement for the oil flow meter, 0.5 SLPM for the air mass flow meter, 0.138 atmospheres (2 psi) for the pressure gauge and 1 °K for the thermocouples.

The mixture of air and ISO VG 2 lubricant flows into the damper film lands through a hole located at the top of the bearing housing. The bubbly lubricant exits the damper through the axial ends, open to ambient conditions. The mixture supply pressure and temperature is nearly ambient. The oil viscosity at room temperature (25°C) is 2.96 cPoise.

Figure 4 portrays the structure supporting the electromagnetic shakers. The structure is made of 38.1 mm (1 ½") square steel bars and rigidly bolted to the table where the test rig resides. An arrangement of elastic ropes (bungee cords) was used to suspend and align the shakers.

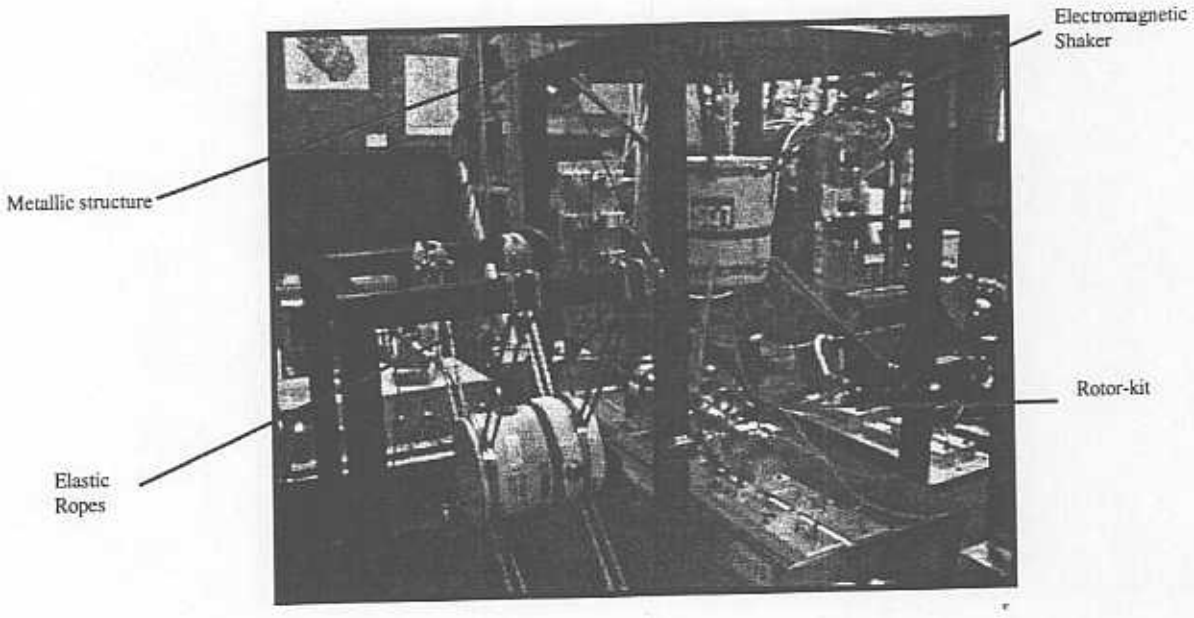

Figure 4. Support structure for shakers.

The stingers were machined from a 10-32 UNF threaded steel bar to a length and diameter equal to 152.4 mm (6") and 4.57 mm (0.18"), respectively. Figure 5 depicts the attachment of the stingers to the squirrel cage and the load cell measuring the force exerted by the shaker.

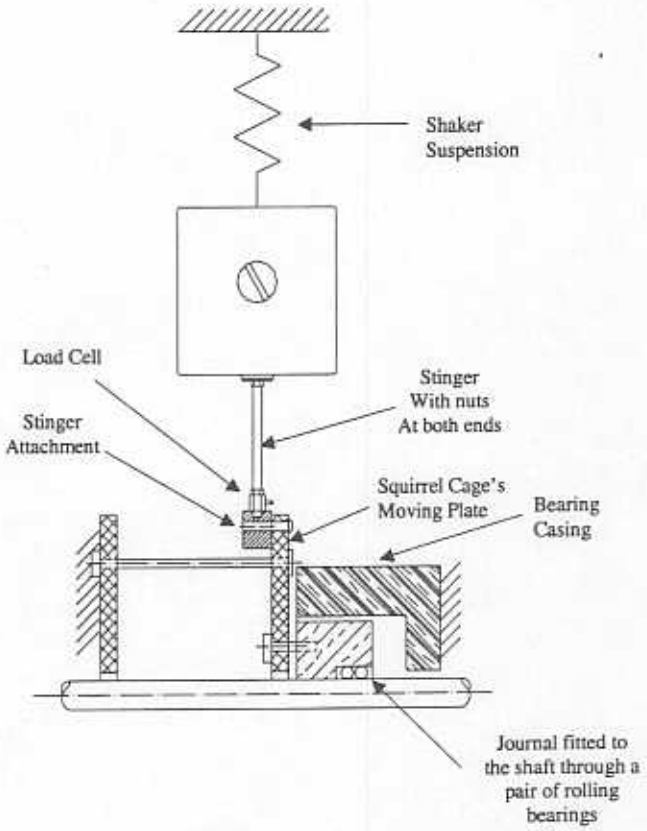

Figure 5. Shaker-Stinger-Squirrel Cage Arrangement.

SYSTEM EQUIVALENT MODEL

The system can be described as a simple spring-mass oscillator for excitation frequencies well below the first elastic mode of vibration. The fundamental mode of vibration is conical as shown in Figure 6.

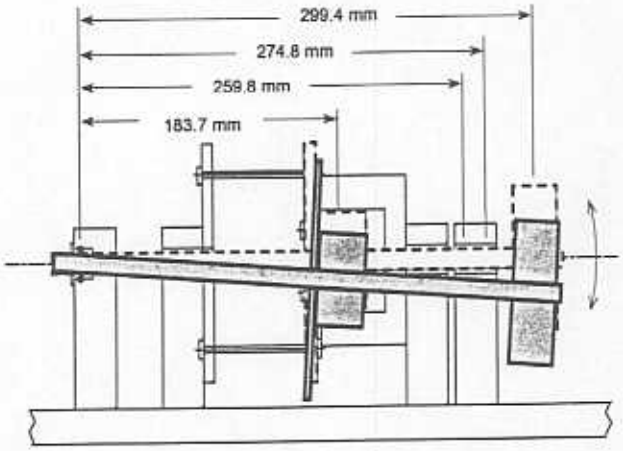

Figure 6. Rotor conical mode of vibration.

Figure 7(a) depicts the physical system with equivalent parameters defined at the *SFD* location. Figure 7(b) shows the equivalent translational linear system. The rotor motion is represented by horizontal and vertical displacements of the shaft centerline at the middle point of the journal. The system dynamic parameters, namely equivalent inertia, stiffness and damping, are identified at this location.

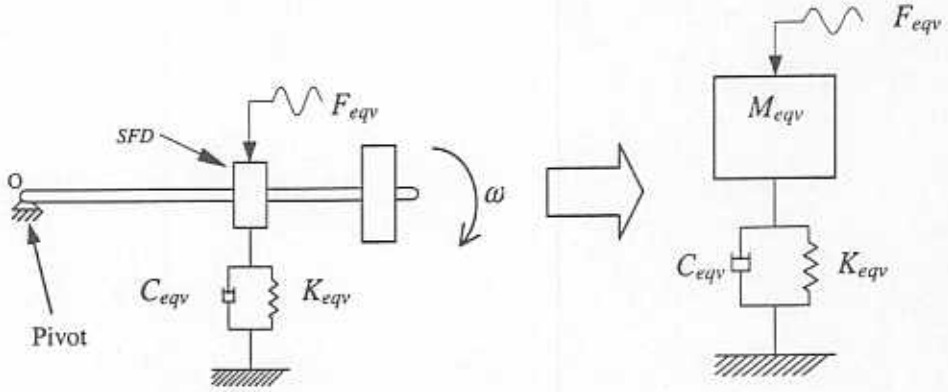

Figure 7 (a) Figure 7 (b)

Figure 7. Equivalent representation of rotor-SFD system.

The equation of motion for the rotor-SFD system describing conical motions is

$$\Sigma M_{ext_o} = I_o \cdot \ddot{\theta} = L_{SFD} \cdot F_{SFD} = L_{Disk} \cdot F_{Disk} \qquad (1)$$

and the kinematical condition,

$$x_{SFD} = 6 \cdot L_{SFD}\,;\; x_{Disk} = 6 \cdot L_{Disk} \qquad (2)$$

reduces equation (1) to

$$\left(\frac{I_o}{L_{SFD}^{\,2}}\right)\ddot{x}_{SFD} + C_{SFD}\dot{x}_{SFD} + K_{SFD}x_{SFD} = F_{SFD}\,, \qquad (3a)$$

or

$$\left(\frac{I_o}{L_{Disk}^{\ 2}}\right)\ddot{x}_{Disk} + C_{Disk}\dot{x}_{Disk} + K_{Disk}x_{Disk} = F_{Disk} \qquad (3b)$$

The relation between the equivalent parameters defined at the disk or SFD location is:

$$F_{Disk} = F_{SFD}\cdot\left(\frac{L_{SFD}}{L_{Disk}}\right) \quad ; \quad M_{SFD} = M_{Disk}\cdot\left(\frac{L_{Disk}}{L_{SFD}}\right)^2$$

$$C_{SFD} = C_{Disk}\cdot\left(\frac{L_{Disk}}{L_{SFD}}\right)^2 \quad ; \quad K_{SFD} = K_{Disk}\cdot\left(\frac{L_{Disk}}{L_{SFD}}\right)^2 \qquad (4)$$

Where $\frac{I_o}{L_{SFD}^{\ 2}} \equiv M_{SFD}$ and $\frac{I_o}{L_{Disk}^{\ 2}} \equiv M_{Disk}$. The nominal equivalent mass (M_{SFD}) coefficient at the *SFD* location is equal to 5.09 kg for both the vertical and horizontal directions. The nominal equivalent stiffness coefficients (K_{SFD}) are $158.8^{\pm 4.9}$ kN/m and $175.1^{\pm 6.1}$ kN/m for the horizontal *(X)* and vertical *(Y)* directions, respectively.

Rotordynamic model of system

A transfer matrix model [13] of the rotor-SFD system allows the prediction of the system undamped natural modes of vibration at low rotational speeds. The stiffness coefficients of the squirrel cage are obtained from static measurements of force and displacement at that location. The stiffnesses are K_{XX}=158.8 kN/m (907 lb/in) and K_{YY}=175.1 kN/m (1000 lb/in). The measured mass of the bushing is $0.144^{\pm 0.002}$ kg. The stiffness of the O-ring [$1.489\cdot10^5 \pm 3.3\cdot10^3$ N/m (850 lb/in)] and the weight of the journal plus the ball bearings [$7.96^{\pm 0.22}$ N (1.79 lb)] are taken from prior measurements [14]. The mass of the support plate holding the squirrel cage and the stingers' attachment parts are estimated from their geometry and equal to 1.641 kg (3.617 lb). The disk mass is 0.811 kg (1.8 lb).

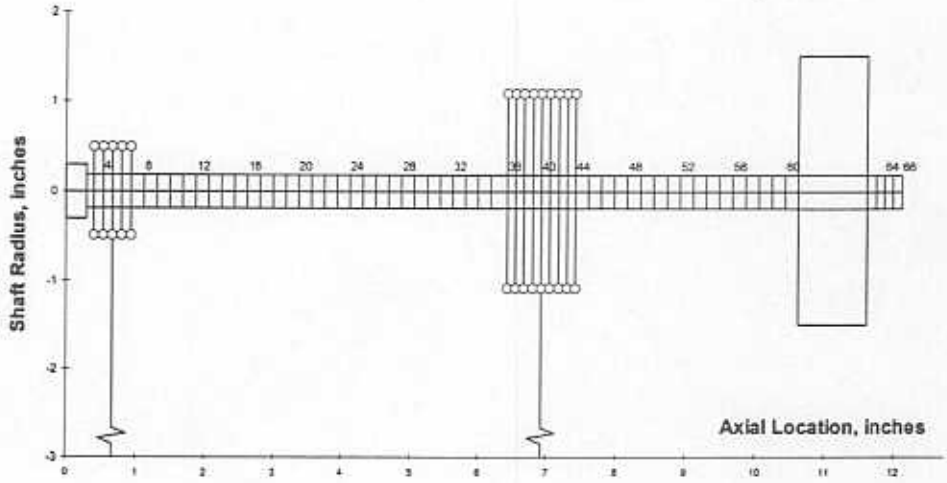

Figure 8. Rotor –SFD transfer matrix model.

Figure 8 shows a schematic view of the stations in the transfer matrix model. The predicted undamped natural frequencies are ω_{1x}=25.9 Hz, ω_{1y}=26.7 Hz, and ω_{2x}=74.8 Hz, ω_{2y}=76.0 Hz for the first two modes of vibration shown in Figure 9. The predicted natural frequencies agree well with measurements, as detailed later.

Design Considerations for the stingers

The selection of the stinger flexural stiffness and shaker support stiffness followed a procedure to reduce the influence of the shaker inertia on the measurements of displacements [12]. Figure 10 shows the predicted transmissibility ratio as a function of excitation frequency using high and low shaker support stiffness. The transmissibility (TR) indicates the isolation of the shaker system from the structure with nil or small values desired so as not to affect the dynamic characteristics of the system under scrutiny.

In Figure 10, a low support stiffness [$2.63 \cdot 10^4$ N/m (150 lb/in)] represented by the continuous line renders a near zero transmissibility for frequencies above 5 Hz. For a high stiffness [$4.38 \cdot 10^5$ N/m (2,500 lb/in)], dashed line, the transmissibility shows a peak at a frequency near 50 Hz, and within the frequency range of interest. In the experiments for parameter identification, a low stiffness value of approximately 9,000 N/m (51.3 lb/in) was obtained using bungee cords to hold the shakers from the structure.

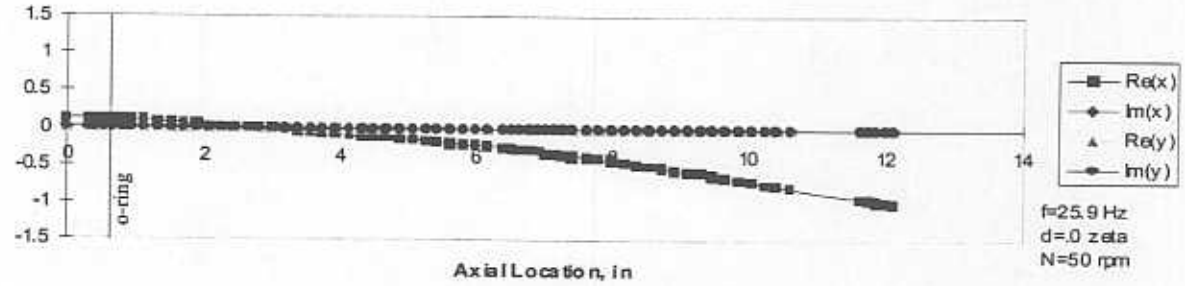

(a) First Mode Shape Plot. Horizontal Direction

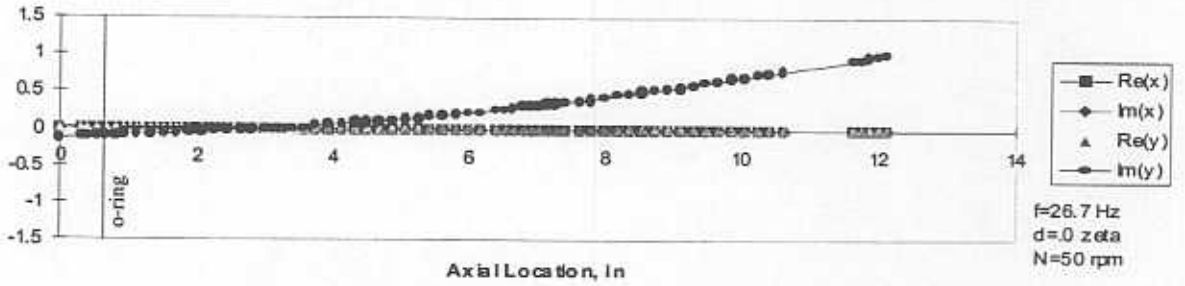

(b) First Mode Shape Plot. Vertical Direction

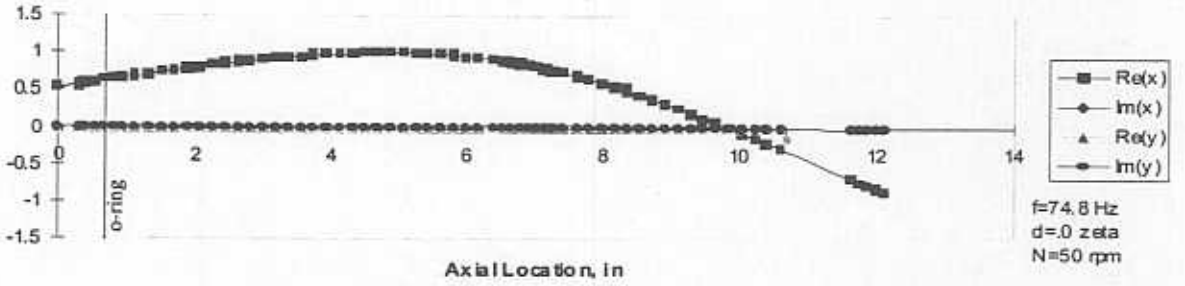

(c) Second Mode Shape Plot. Horizontal Direction

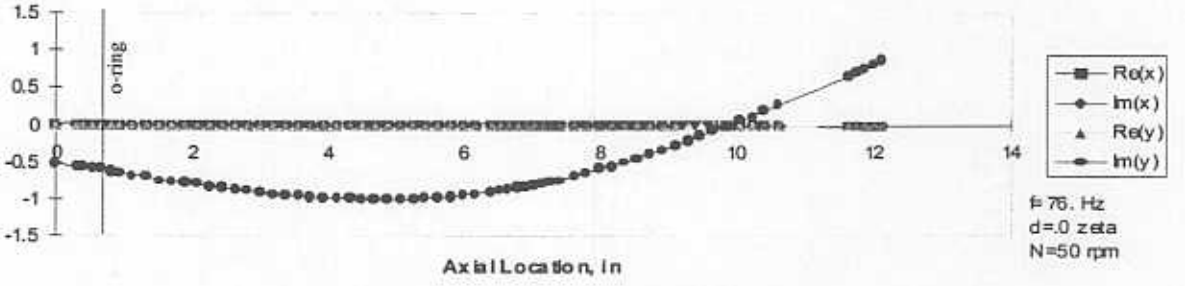

(d). Second Mode Shape Plot. Vertical Direction.

Figure 9. Predicted mode shapes for rotor-SFD system.

Validation of Stingers Design.

Rap tests on the rotor were performed to verify the negligible influence of the shaker inertia on the dynamic behavior of the system. The recorded natural frequencies with the stingers attached and shakers in place were 29.6 and 28.0 Hz in the vertical and horizontal directions, respectively. These frequencies of nearly identical magnitude as those for the system alone demonstrate the convenience of the stingers and shaker support arrangement implemented.

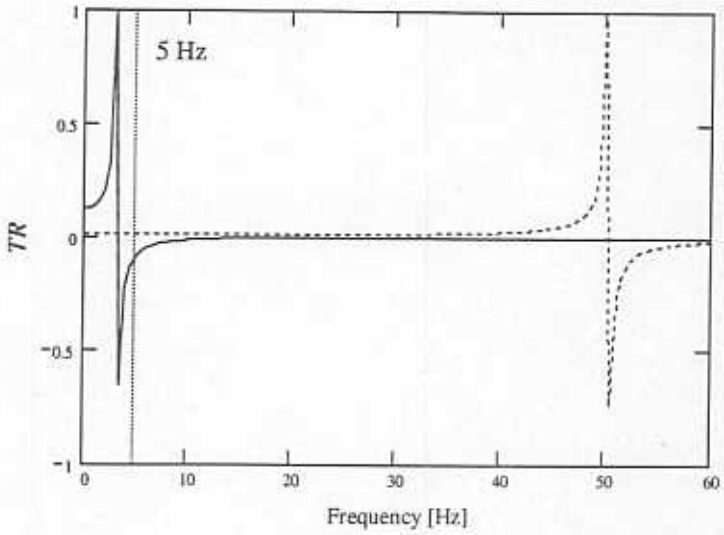

Figure 10. Transmissibility for high (dashed line) and low (solid line) shaker support stiffness.

EXPERIMENTAL PROCEDURE

Measurements of the *SFD* squirrel cage stiffness.

The stiffness of the *SFD* elastic support (squirrel cage) in two lateral directions, (K_{xx}, K_{yy}), was determined by applying known static forces and measuring the corresponding displacements with a dial gauge. Figure 11 depicts the load (F_i) versus deflection ($X,Y)_i$ results for the tests in the horizontal (X) and vertical (Y) planes. For simplicity, and given the smallness of the cross coupled displacements, no attempt was performed to measure cross coupled force coefficients.

The stiffness corresponds to the system equivalent stiffness at the *SFD* location and obtained from the slope of the straight line best fitting the measurements [15], i.e.

$$K = \frac{N\sum X_i F_i - \sum X_i \sum F_i}{N\sum\left(X_i^{\,2}\right) - \left(\sum X_i\right)^2} \qquad (5)$$

The identified stiffnesses are equal to K_{xxs}= 158.8$^{\pm 4.92}$ kN/m and K_{yys}= 175.1$^{\pm 6.07}$ kN/m in the vertical and horizontal directions, respectively.

A novel procedure is introduced to estimate the uncertainty of the measured stiffness. Note that the stiffness is not measured directly nor it is obtained from an algebraic relation between the measured parameters. The stiffness $K=f(X_1,X_2,...,X_N,F_1,F_2,...F_N)$ is estimated from a least squares curve fit best representing the measurements. This condition prevents direct application of the conventional uncertainty formulae to the simple relationship $K=F/X$. In the tests, the uncertainties in displacements is 0.013 mm ($0.5\cdot10^{-3}$ in) and in forces is 2.22 N (0.5 lb).

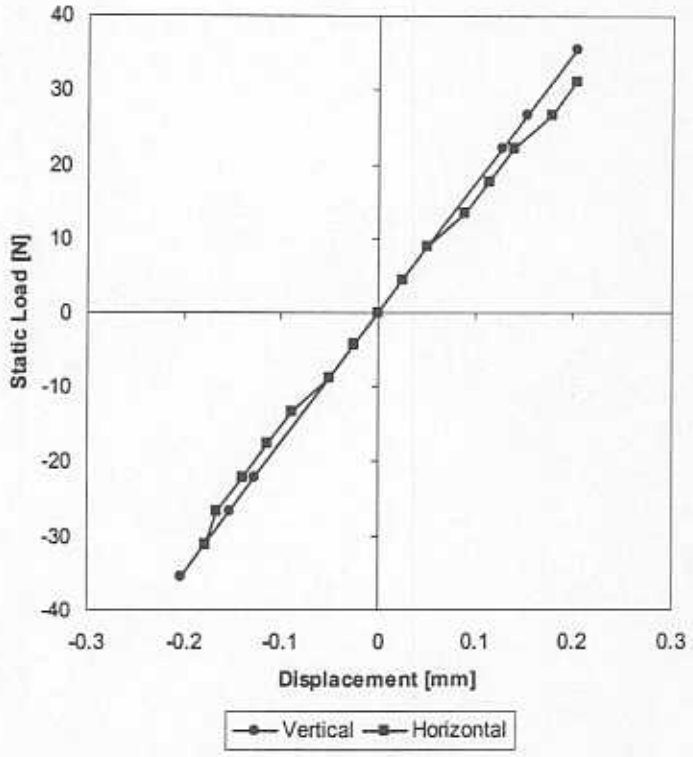

Figure 11. Static load vs. displacement measurements to estimate the squirrel cage stiffness.

The uncertainty in the stiffness (U_K) is determined by a standard Kline-McClintock [16] error propagation analysis applied to equation (5). The resulting formulae are:

$$U_K = \left(\sum_{i=1}^{N} \left(\frac{\partial K}{\partial X_i} U_{X_i} \right)^2 + \sum_{i=1}^{N} \left(\frac{\partial K}{\partial F_i} U_{F_i} \right)^2 \right)^{\frac{1}{2}} \qquad (6)$$

$$\frac{\partial K}{\partial X_i} = \frac{\left(N\sum(X_j)^2 - \left(\sum X_j\right)^2\right)\cdot\left(N\cdot F_i - \sum F_j\right) - \left(N\cdot\sum F_j\cdot X_j - \sum X_j\cdot\sum F_j\right)\cdot\left(2\cdot N\cdot X_j - 2\cdot\sum X_j\right)}{N\cdot\sum X_j^{\,2} - \left(\sum X_j\right)^2} \qquad (7)$$

$$\frac{\partial K}{\partial F_i} = \frac{N\cdot X_i - \sum X_j}{N\cdot\left(\sum X_j^{\,2} - \left(\sum X_j\right)^2\right)} \qquad (8)$$

where (U_i) represents the uncertainty of each measured variable (displacement or force).

Validation of predicted mode shapes.

Rap tests on the rotor were conducted to measure the mode shapes of vibration and comparison with the model predictions. A piezoelectric impact hammer hits the rotor at the disk location and shaft vertical accelerations are recorded at two locations. The position of one accelerometer is fixed at a reference location while the other one is varied along the axis of the rotor. The vibration signals are recorded in the frequency domain and presented as the ratio of magnitudes.

Figure 12 depicts the magnitude of acceleration ratios for the first and second natural frequencies versus the location of measurement. The predicted mode shapes from the model are also included in the figure. The measured natural frequencies are $\omega_{1x}=30.5^{\pm 0.25}$ Hz and $\omega_{2x}=61.4^{\pm 0.73}$ Hz. The differences in the prediction of the natural frequencies are 12.5% and 19.2%, for the first and second modes, respectively. The mode shape predictions closely match the measurements and validate the characterization of the rotor-*SFD* system as a simple 1 DOF system. Furthermore, the eddy-current displacement sensors were relocated near the nodal point of the second mode to reduce their influence on the parameter identification experiments

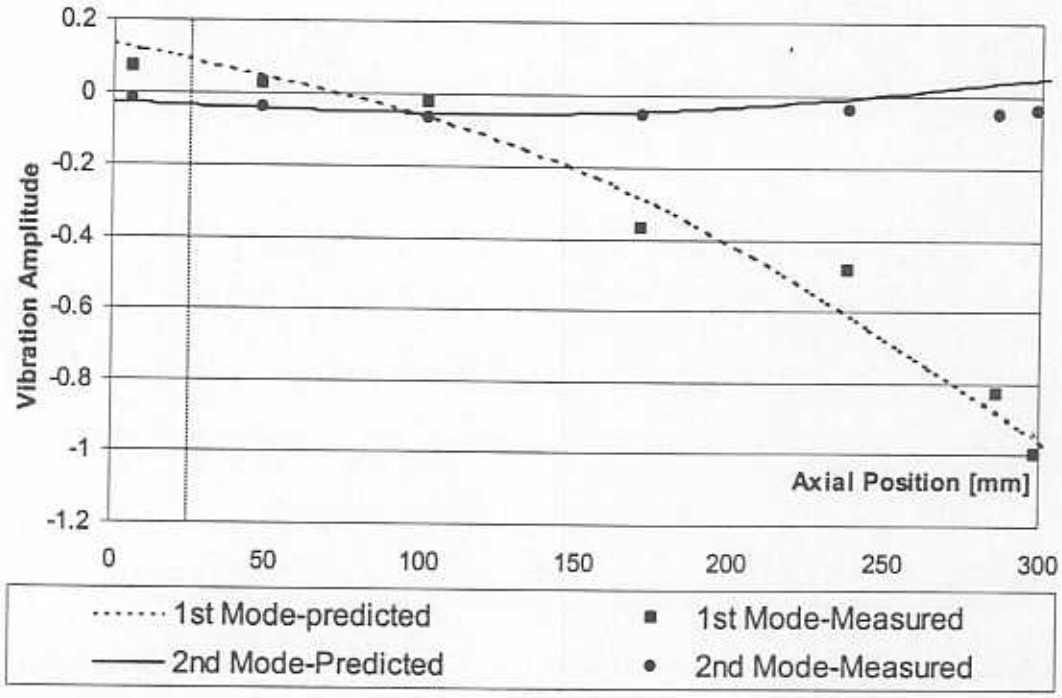

Figure 12. Predicted and measured modes of vibration of rotor-SFD system at zero rpm.

EXPERIMENTS WITH SINE SWEEP EXCITATIONS AND CONTROLLED OIL-AIR MIXTURES

A controlled mixture of air and ISO VG 2 oil flows to the *SFD* through a small hole located at the top of the bearing housing. The lubricant exits the test section through both ends open to ambient conditions. The mixture supply pressure and temperature are close to ambient conditions (within ±0.068 bar [1 psi] and ± 1 °C). The mixture is generated in a sparger element installed at the connection of the air and oil lines. The proportions of air and oil are accurately regulated with valves installed in each feed line.

The air volume fraction (λ) of the mixture into the damper is the ratio of measured air volumetric flow to total (air + oil) volumetric flow rate. The air volume fractions range from 0 (pure oil) to 1 (pure air). The size of the bubbles is estimated to range from 0.1 mm to 0.75 mm.

The air temperature at the inlet line, the air mass flow and the oil flow rate are measured to find air volume fractions referred to ambient conditions. The volume fraction uncertainty follows the standard Kline-McClintock error propagation [16] from the instruments measurement uncertainties, i.e.

$$\lambda = \frac{\left(Qair\frac{Po}{P}\frac{T}{To}\right)}{\left(Qair\frac{Po}{P}\frac{T}{To}\right)+Qoil} = \frac{1}{1+\frac{Qoil}{\left(Qair\frac{Po}{P}\frac{T}{To}\right)}} = \frac{1}{1+\frac{Qoil}{Qair}\frac{P}{Po}\frac{To}{T}} \tag{9}$$

$$U_\lambda = \frac{PoTo}{(QairT\cdot Po+Qoil\cdot P\cdot To)^2}\sqrt{(P\cdot T\cdot Qoil\,\delta Qair)^2+(QairP\cdot Qoil\,\delta T)^2+(QairT\cdot Qoil\,\delta P)^2+(QairT\cdot P\cdot \delta Qoil)^2} \tag{10}$$

Refer to the Nomenclature for the designation of the variables above.

Electromagnetic shakers excite the rotor in the vertical and horizontal directions. The electric signal driving the shaker is a constant amplitude sinusoidal wave with a linear time-dependent frequency ranging from 5 to 60 Hz. The sine sweep signal and the frequency range were chosen upon considerations such as shaker transmissibility and the rotor modes of vibration.

The sweep sine force signal repeats three times before the data acquisition triggers and to obtain a system response with negligible effects of initial conditions. The data acquisition system then captures the signals from the load cells and the eddy-current displacement sensors in time domain for the different air volume fractions.

The measurements of displacements are performed at locations L_x and L_y and converted to equivalent displacement at the *SFD* location where the force is applied. The procedure obviously assumes a conical mode of vibration. Figure 13 depicts typical measurements of time responses and their *FFTs* for the shaker force in the horizontal (*X*) direction, and vertical *(Y)* and horizontal *(X)* rotor displacements when a 51.1% air volume fraction mixture flows into the damper. Cross-coupling effects appear to be negligible in most experiments. The observed remaining cross-coupling effects can be attributed to a small asymmetry of the *SFD* squirrel cage, since they are present even when the system is excited with no lubricant in the damper clearance.

Figure 14 displays the response measurements due to an impact load excitation. These results were obtained in a prior investigation conducted with the same test apparatus and for an air volume fraction of 8.6% [8].

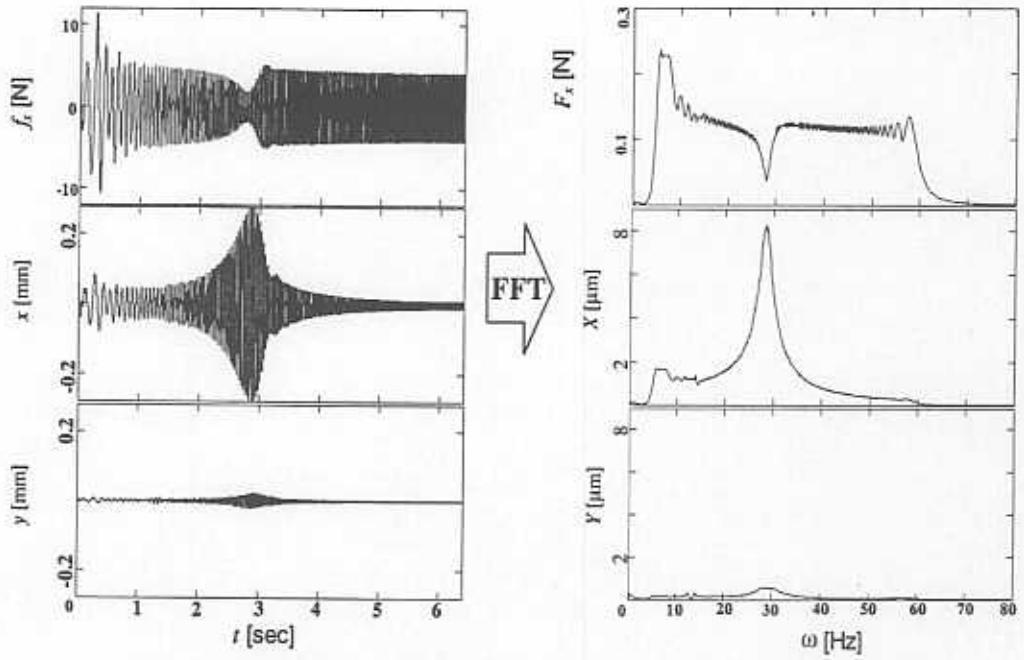

Figure 13. Sine sweep excitation: typical time responses and FFTs

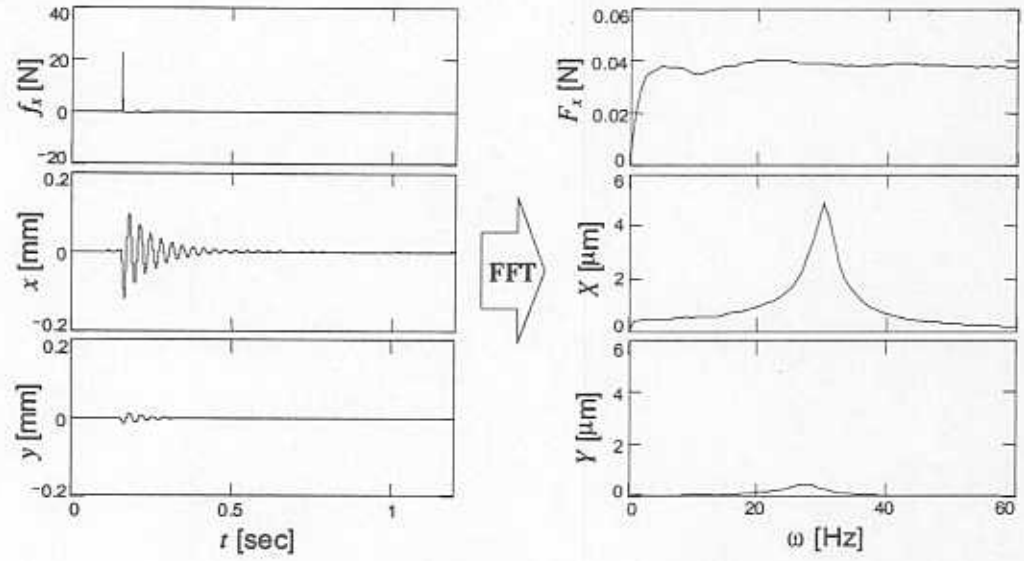

Figure 14. Impact excitation: typical time responses and FFTs

Figures 13 and 14 show the differences on the rotor forced motion when subjected to impact or sine sweep load excitations. In the sine sweep tests, the excitation frequency range is restricted to the range of 5 to 60 Hz, thus avoiding the likeliness of exciting higher rotor modes of vibration and reducing the influence of the shaker inertia on the system dynamic response. The sweep sine load produces high amplitudes of vibration over the whole test time window. Yet, an impact renders smaller amplitudes of vibration for shorter periods of time. As will be verified later, these differences decisively affect the identified damping coefficients.

RESULTS AND DISCUSSION

The dynamic measurements of sine sweep force and displacements were processed with the Instrumental Variable Filter (*IVF*) method for parameter identification in the frequency domain [8,9]. The *FFTs* of the horizontal and vertical shaft displacements for forced excitations in each direction were used to evaluate the impedance matrix at each frequency component. In the identification procedure an average of ten impedance measurements was used for each air-oil mixture. As an example, Figure 15 depicts measured and predicted (curve fits) flexibilities for a mixture with 51% air volume fraction.

The identification frequency ranges from 23.4 Hz to 39.1 Hz. This range includes the system

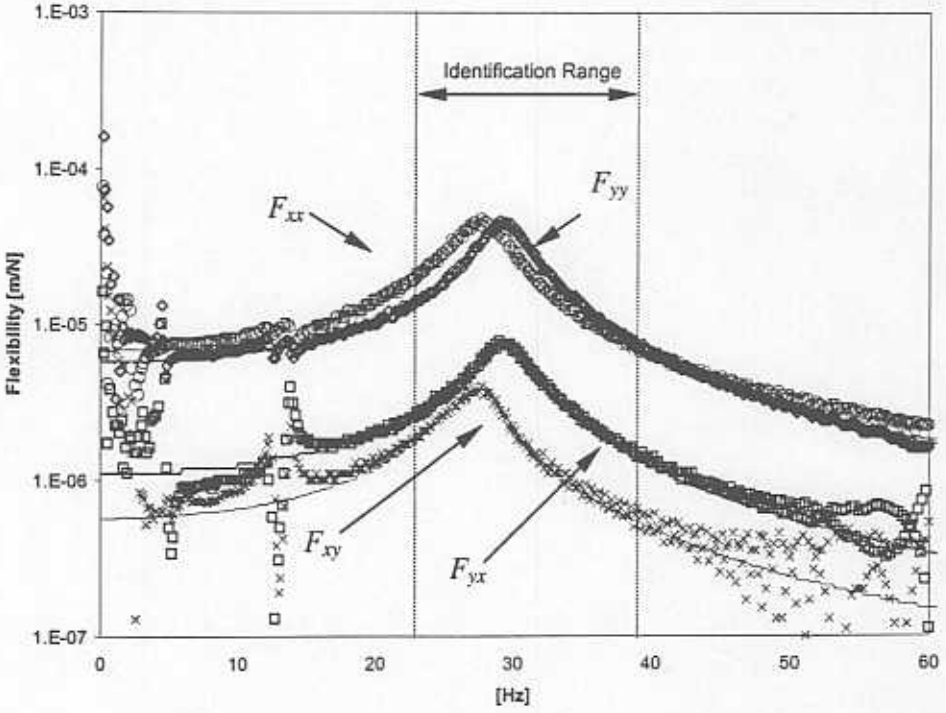

Figure 15. Measured and predicted flexibilities for test with 51% of air volume fraction.

fundamental natural frequency, and excludes those frequencies where the amplitudes of motion were too small, thus avoiding further difficulties with too small signal to noise ratios.

The variability of the estimated parameters as a function of the selected frequency range is of importance to assess the reliability of the identification procedure. Appendix 1 lists the estimated coefficients for the experiments with 51% air volume fraction and increasing frequency ranges. The results show little variation, less than 2.5%, in the estimated coefficients for frequency ranges from 7.8 to 54.7 Hz. A larger frequency range to 78 Hz does show larger percentile variations; however, recall that the maximum frequency in the load function is just 60 Hz. Within the identification frequency range of 23.4 to 39.1 Hz, the correlation factors of the direct and cross-coupled flexibilities are r_{xx}=0.998, r_{xy}=0.999, r_{yx}=0.997 and r_{yy}=0.999. The correlation factor is an indicator showing the goodness of the predicted flexibilities evaluated with the identified parameters to the experimental data. Appendix 2 includes graphs depicting the experimental flexibilities for other air volume fractions.

The identified direct and cross-coupled stiffnesses for increasing air volume fractions in the bubbly mixture are depicted in Figure 16. The average stiffness values and their maximum percent variation are K_{xx}=149.8 kN/m (2.3%), K_{yy}=180.3 kN/m (2.3%), K_{xy}=-28.9 kN/m (4.9%) and K_{yx}=-15.5 kN/m (11.8%). The identified direct stiffness values are virtually independent of

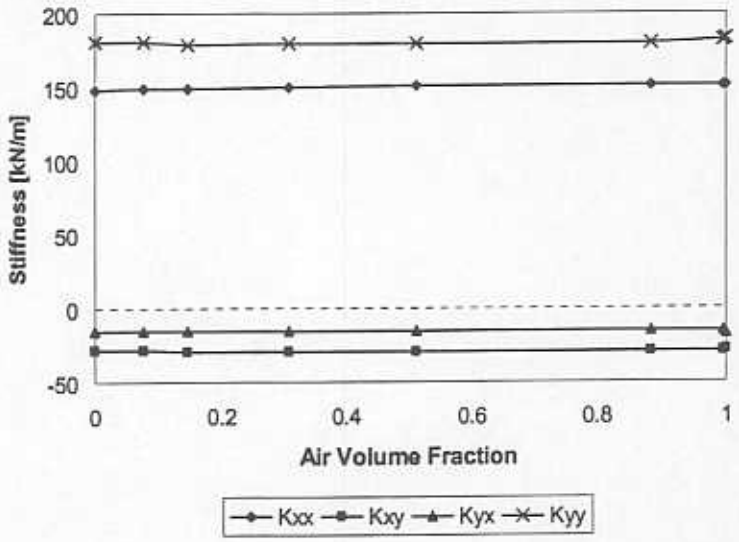

Figure 16. Stiffness coefficients identified from sine sweep excitation tests.

the air volume fraction and correlate well with those derived from the static measurements, i.e. K_{xxs}=158.8$^{\pm 4.9}$ kN/m (907$^{\pm 28}$ lb/in) and K_{yys}=175.1$^{\pm 6.1}$ kN/m (1,000$^{\pm 35}$ lb/in). Differences of -6% and +3% in the horizontal and vertical stiffnesses are determined in relation to their static counterparts. These results evidence that (a) the active *SFD* does not contribute to the stiffness of the system, and (b) the IVF identification method renders highly reliable stiffness coefficients.

The estimated cross-coupled stiffnesses are not nil as assumed in the static analysis. The values, although one order of magnitude less that the direct stiffness coefficients, cannot be regarded as negligible. The identified cross-coupled stiffnesses evidence the small structural asymmetry in the SFD elastic support. Note that both cross-stiffness are of similar magnitude and have a negative sign.

Figure 17 shows the inertia coefficients derived from the sweep sine excitation tests for increasing air volume fractions. The identified inertias show little variation with the air/oil mixture content, with average values and maximum percent variation equal to M_{xx}=4.99 kg (2.5%), M_{yy}=5.31 kg (2.7%), M_{xy}=-0.96 kg (3.8%) and M_{yx}=-0.45 kg (11.7%). The estimated equivalent inertia based on the system geometry and material properties renders a value equal to M_{xx}=M_{yy}=5.09 kg and zero cross-coupled values. Differences of -2% and +4.3% in the horizontal

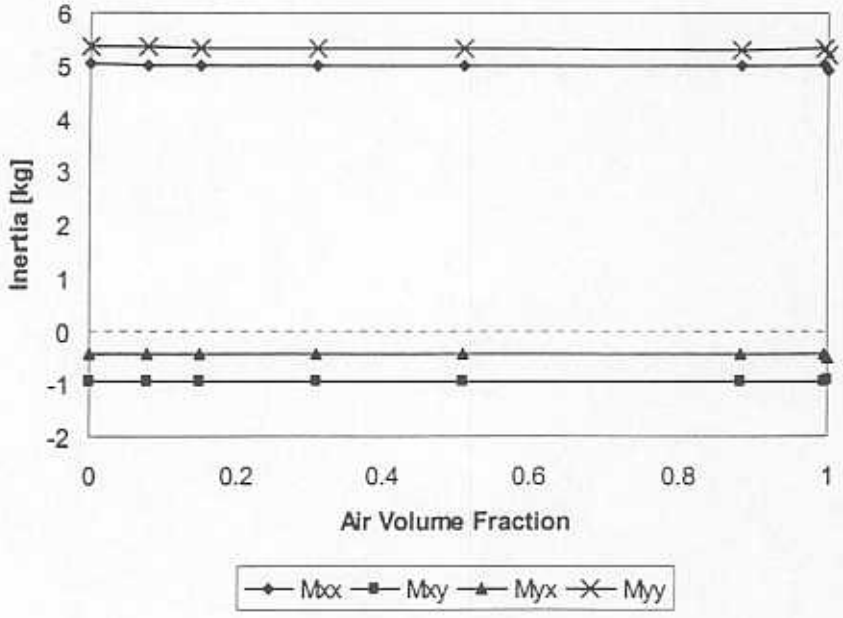

Figure 17. Inertia coefficients identified from sine sweep excitation tests.

and vertical inertia coefficients are determined in relation to the inertia based on the system geometry. Note that fundamental natural frequencies based on the estimated direct stiffness and inertia coefficients are equal to 29.3 Hz and 27.8 Hz in the vertical and horizontal directions, respectively. These values agree closely with those measured experimentally, i.e. 29.6 and 28.0 Hz.

Figure 18 shows the equivalent damping coefficients estimated from the sweep sine excitation tests for increasing air volume fractions. The identified damping coefficients, direct and cross-coupled, show little variation with the air/oil mixture content, except for the pure oil and pure air conditions. Predicted *SFD* damping coefficients for the pure oil condition, centered journal and considering a full film extent (no cavitation) are given by [8]:

$$C_{XX} = C_{YY} = 12\,\pi\,\mu\,L\left[\frac{R}{c}\right]^3\left(1-\frac{tgh(L/D)}{(L/D)}\right) = 137\ N.s/m; \qquad (11)$$
$$C_{XY} = C_{YX} = 0$$

The measured lubricant viscosity equal to 2.80 cPoise at room temperature (30°C) is used in the formula above. The predicted direct damping magnitude shows a difference of 7.7% and

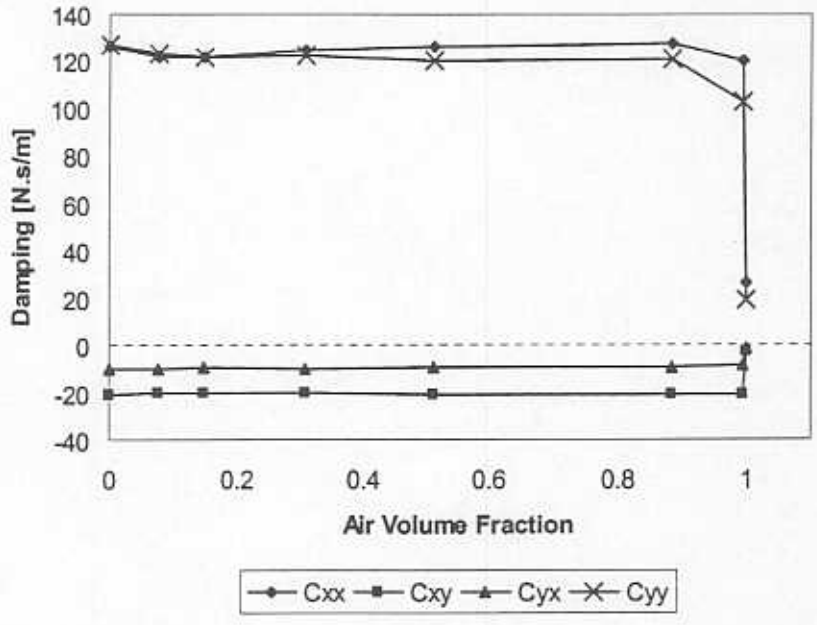

Figure 18. Damping coefficients identified from sine sweep excitation tests.

6.6% with the identified horizontal and vertical direct damping coefficients. Note that the identified cross-coupled damping coefficients are small, and may further evidence a structural asymmetry.

Table 1 shows the damping coefficients identified with the *IVF* method in the sine sweep excitation tests for different air volume fractions.

Table 1. Damping coefficients versus volume fractions derived from sine sweep load experiments.

λ volume fraction	C_{xx} [N.s/m]	C_{yy} [N.s/m]	C_{xy} [N.s/m]	C_{yx} [N.s/m]
0	126.06	127.06	-21.07	-10.02
0.078	121.77	123.59	-20.02	-9.76
0.148	121.96	121.46	-20.12	-9.55
0.309	124.98	122.66	-20.60	-9.77
0.511	126.51	120.60	-20.70	-9.53
0.884	127.79	121.26	-21.28	-9.56
0.995	120.37	102.87	-20.70	-8.37
1	26.39	19.06	-2.82	-1.29

Comparison of force coefficients derived from sweep sine and impact excitations

The system parameters identified from impact excitations on the same test rig [8, 17] are compared with the ones derived from the sine sweep load experiments. Table 2 presents the average direct stiffness and inertia coefficients obtained from the impact and sweep sine excitations, along with the statically estimated values. Inspection of the coefficient magnitudes and their uncertainties evidences that the excitation method has no notable influence on their reliable estimation.

Table 2. Average direct stiffness and inertia coefficients derived from impact and sweep sine load experiments and static measurements

Average	M_{xx} [kg]	M_{yy} [kg]	K_{xx} [kN/m]	K_{yy} [kN/m]
Sine Sweep	$4.99^{\pm 0.13}$	$5.31^{\pm 0.14}$	$149.80^{\pm 3.5}$	$180.28^{\pm 4.1}$
Impact [8]	$5.22^{\pm 0.27}$	$5.29^{\pm 0.57}$	$161.95^{\pm 16.9}$	$187.22^{\pm 16.5}$
Static	5.09	5.09	$158.80^{\pm 4.9}$	$175.1^{\pm 6.1}$

Figure 19 depicts the identified direct damping coefficients extracted from the impact and sine-sweep load experiments versus increasing air volume fractions. Similar damping coefficients are obtained for the pure oil (λ=0) irrespective of the excitation type. However, for most air volume fractions there are distinct differences in the estimated damping coefficients and apparently due to the type of force excitation exerted on the system. For the impact tests, the identified damping coefficients increase as the air volume fraction increases to about 50 %, and

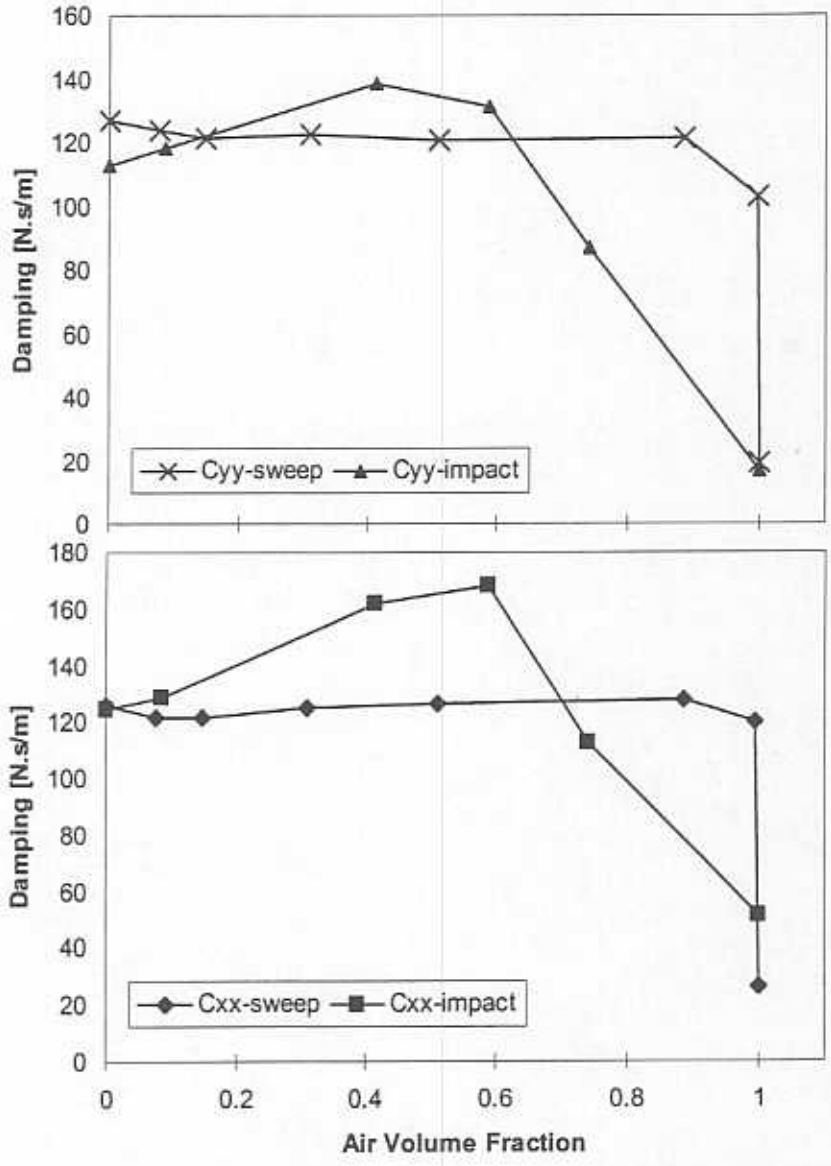

Figure 19. Direct damping coefficients identified from impact and sine sweep load excitations.

then rapidly decrease with a raise in the air volume fraction [8]. On the other hand, the damping coefficients extracted from the sine sweep excitations are nearly constant though lower than the coefficients derived from the impact tests for air volume fractions up to 60 %. Most notably, the sweep sine derived damping coefficients remain invariant even for larger inlet air volume fractions while the coefficients derived from impacts drop sharply with further increases in the air content of the mixture.

Arguments based on sound physical descriptions must adequately address to the discrepancies found in the identified damping coefficients. Recall that the test *SFD* has a large clearance (0.290 mm) and lubricant cavitation (vapor or gaseous) is implausible even for large amplitude journal motions. The damping coefficients derived from the impact tests appear to indicate an increase in the effective viscosity of the lubricant mixture for small air volume contents. Note that the intrinsic nature of the impacts generates too fast transient responses (see Figure 14) that may prevent the mixture compressibility from affecting the generation of film pressures and the *SFD* damping coefficients [8].

For both types of forced excitations (impact and sine sweep), it is likely that air in the mixture is expelled from the film earlier than the oil, thus resulting in a lubricant with a lower air content than the one measured at the supply condition. However, in the sweep sine load tests, the amplitudes of motion are rather large, up to 80% of the radial clearance. Recall that the axial fluid velocity at the damper exit plane (V_z) is proportional to the amplitude of motion (A) and the excitation frequency (ω), i.e.

$$V_z = \lambda \left(A\omega \frac{L}{2C} \right) \frac{1}{\left[1-(A/C)^2\right]^{1/2}} \qquad (12)$$

When the amplitudes of motion are small relative to the damper clearance, the bubbles in the mixture may not be readily compressed and behave as rigid particles, thus increasing the mixture effective viscosity and rendering increased damping coefficient. This type of results was found from the impact tests for volume fractions as large as 50% [8].

On the other hand, in the sweep sine load tests the journal amplitudes of motion are large and well above 50% of the damper clearance, in particular while traversing the system natural frequency (see Figure 13). A simple calculation using equation (12) shows that for journal

motions at the system natural frequency (ω~29 Hz), the axial fluid speed is equal to (0.47 λ m/s) and (3.08 λ m/s) for dynamic motions with amplitudes (A) equal to 20% and 80% of the radial clearance, respectively. Thus, the larger the amplitude of motion the higher the fluid speed leaving the damper. Then, it is likely that the air bubbles within the lubricant are rapidly propelled out of the film due to the sustained harmonic motions of large amplitude, and render a mixture of low local volume fraction (i.e., pure lubricant) at the position where the journal motion is most prevalent.

The reasoning then shows that, for the sweep sine load induced journal motions, minute (discrete) amounts of pure lubricant, filling the clearance at those locations where the squeeze velocity exerts its action, are enough to produce damping coefficients of the same magnitude as in a damper with a full liquid film. Prior experimentation at the laboratory has shown that a few drops of lubricant are enough to produce commensurate viscous damping coefficients[2].

It is important to note that the highest volume fraction mixtures showed bubbles of large size (about 2 mm in diameter) which were rapidly expelled from the film due to the combined actions of the journal motion, the small axial pressure gradient insuring adequate flow, and buoyancy effects. Thus, these large bubbles probably never reached the sides and bottom clearances in the damper. The reported volume fraction corresponds to the supply conditions, but the actual one within the damper lands must have been lower. Note that this effect is rather small for low to moderate volume fractions since the mixture supplied appeared to be homogeneous.

Earlier investigations conducted in another *SFD* test rig performing circular centered orbits and fed with a homogeneous bubbly mixture show that the direct damping coefficient steadily decreased with the air volume fraction[3] [3, 6, 7]. Dynamic pressure measurements and flow visualization [18] evidence the formation and permanence of a (non homogenous) large gas cavity of uniform pressure and rotating synchronously with the whirl orbit. The cavity grows in extent as the mixture volume fraction increases thus preventing the generation of squeeze film

---

[2] The identification of system parameters under dry (no lubricant) conditions has been constant in our experimental research program. Numerous times, experimental damping coefficients for dry conditions have shown similar magnitudes to the "wet" ones, i.e. with the lubricant filling the annular clearance. Further work evidenced that the "dry" dampers still contained a few drops of lubricant and thus provided significant viscous damping to the test system.

[3] The diameter (D), length (L) and clearance (c) of the test damper are 191.1 mm, 31.1 mm and 0.343 mm, respectively. The (c/R) ratio equals 0.0053.

pressures, and consequently reducing the damping forces. In those experiments, dynamic pressures on the order of 2 bars were recorded for whirl frequencies to 100 Hz.

Recall that the present sweep sine force experiments have been conducted on a small-scale test rig (c/R=0.023) and the expected magnitudes of dynamic pressures are on the order of 0.2 bars for the loads exerted on the system. Thus, the induced hydrodynamic pressures generated by the journal harmonic motion are not low enough to produce the coalescence of small bubbles into an enlarged cavity. In actuality, as detailed above, the largest bubbles in the mixture appear to be propelled out of the film, thus leaving a local fluid film region with a lower volume fraction.

Thus, the damping force coefficients derived from the sweep sine load tests further evidence that the journal kinematics decisively affects the flow (shape and motion) of the air bubbles and ultimately determine the *SFD* reaction forces.

Experiments with single frequency force excitations

Further experiments were conducted with single-frequency force excitations. These tests aimed to verify the trends observed in the sweep sine experiments. Appendix 3 summarizes the experiments and results obtained for increasing air volume fractions. Three single frequencies were selected, corresponding to values below, above and around the system natural frequency, for vertical and horizontal direction.

Figure 20 depicts the magnitude and phase of the measured direct flexibilities or (F_{xx}, F_{yy}) in the vertical and horizontal directions for a test conducted with a mixture of 50% air content. The continuous lines represent the measured flexibility magnitude and phase obtained from the sweep sine tests, and the symbols denote the values obtained from the single frequency excitation experiments. In general, the results of the single frequency experiments correlate very well with the sine sweep excitation derived results.

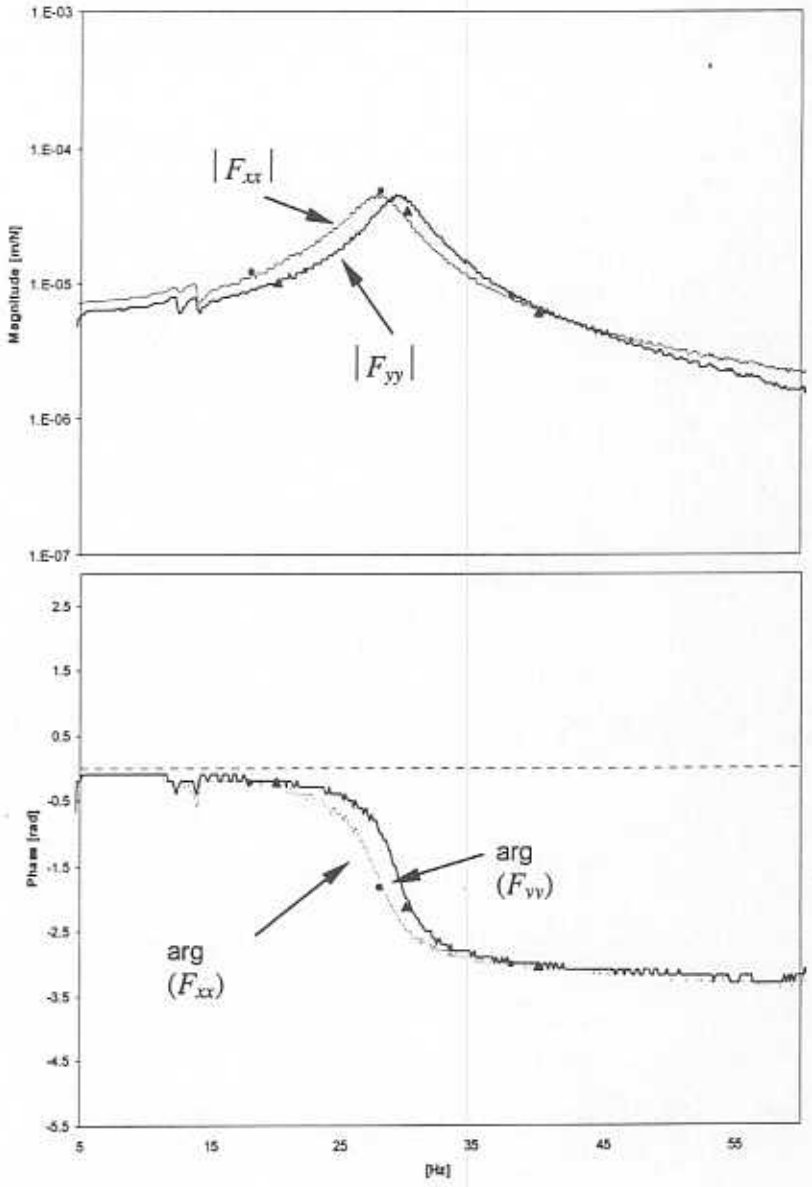

Figure 20. Measured flexibilities (magnitude and phase) for sine sweep and harmonic excitation tests with mixture 50% air volume.

CONCLUSIONS

Experiments using sweep sine load excitations were conducted to identify the force coefficients in a small rotor-*SFD* system. The *SFD* operated with a controlled bubbly mixture generated by mixing air and lubricant in a sparger element. The rotor-*SFD* is modeled as a single DOF system for the range of frequencies used in the experiments. A complete characterization of the rotor system and the shaker structure were necessary to validate the procedure and major assumptions.

The force coefficients were extracted using the Instrumental Variable Filter method for measurements of the load and rotor displacements in the frequency domain. The derived equivalent direct stiffness and inertia force coefficients agree well with independent static measurements and are not affected by the air content in the bubbly lubricant mixture. The experiments also revealed a small degree of structural cross coupling.

The identified coefficients derived from the sweep sine load experiments differ dramatically with those determined earlier from the transient response due to impact loads. Presently, the direct damping coefficients are nearly constant and not affected by the condition of the bubbly lubricant even for large volume concentrations of air in the mixture. Force coefficients determined from the impact tests, on the other hand, showed an increase for volume fractions up to 50% due to the fastness of the transient rotor motions and the bubbles acting as rigid particles within the mixture.

In the sine sweep experiments, the large amplitudes motion of the damper journal due to the sustained periodic load excitation appear to expel rapidly the air bubbles thus rendering locally a mixture of less air content that that fed at the supply port. This process then leads to the generation of similar dynamic pressures and damping force coefficients.

The complexity of the bubbly flow mechanics in squeeze films is currently investigated in another test rig. Flow visualizations with image identification techniques to determine the path of the gas bubbles and striations will aid to elucidate further the phenomena observed. Until those results are available, it becomes essential to note that *SFDs* operating with bubbly mixtures show a forced performance that depends greatly on the type of excitation induced.

REFERENCES

1. Edney, S. L. and Nicholas, J.C., "Retrofitting a Large Steam Turbine with a Mechanically Centered Squeeze Film Damper," Proceedings of the 28TH Turbomachinery Symposium. Pages 29-40, (1999).
2. Vance, J. M., "Rotordynamics of Turbomachinery," John Wiley and Sons Pubs, NY (1988).
3. Diaz, S.E. and San Andrés, L.A., "Reduction of the Dynamic Load Capacity in a Squeeze Film Damper Operating with a Bubbly Lubricant," ASME 98-GT-109.
4. Zeidan, F.Y., San Andrés, L.A., and Vance, J.M., "Design and Application of Squeeze Film Dampers in Rotating Machinery," Proceedings of the 25TH Turbomachinery Symposium, Pages 169-188. (1996).
5. Zeidan, F. Y. and Vance, J. M., "Cavitation Regimes in Squeeze Film Dampers and their Effect on the pressure Distribution," STLE Tribology Transactions, Vol. 33, pp 447-453.
6. Diaz Briceño, Sergio, "The Effect of Air Entrainment on the Performance of Squeeze Film Dampers: Experiments and Analysis," PhD Dissertation, Texas A&M University, May (1999).
7. Diaz, S. and San Andrés, L.A., "Air Entrainment Vs. Lubricant Vaporization in Squeeze Film Dampers: An Experimental Assessment of the Fundamental Differences," ASME Paper 99-GT-187, IGTI ASME TurboEXPO, Indianapolis, IN, June 1999.
8. Diaz, S. E. and San Andrés, L. A., "A Method for Identification of Bearing Force Coefficients and Its Application to a Squeeze Film Damper with a Bubbly Lubricant," Tribology Transactions. Vol. 42 (1999), 4, 739-746.
9. Fritzen, C., "Identification of Mass, Damping and Stiffness Matrices of Mechanical Systems," ASME Paper 85-DET-91, (1985).
10. Diaz, S.E., "Experimental Parameter Identification of a nxn Linear System, "Internal Research Progress Report, Rotordynamics Laboratory, Texas A&M University, College Station, TX, (1997).
11. Hewlett Packard, "The Fundamentals of Modal Testing," Application Note 243-3, Pages 18-21.
12. Mitchell, L.D. and Elliot, K.B., "How to Design Stingers for Vibration Testing of Structures", Sound and Vibration, Pages 14-18. April 1984.
13. Murphy, B. T., "XLROTOR" Rotating Machinery Analysis Inc., Austin, Texas.

14. Laos, H. E., "Measurements of Unbalance Response in a Squeeze Film Damper Test Rotor-Kit," MS Thesis, Texas A&M University, (1995).
15. Coleman, H. W. and Steele, W. G.., "Experimentation and Uncertainty Analysis for Engineers," John Wiley and Sons Pubs, New York, 1989.
16. Kline, S.J., and McClintock, F.A., "Describing Uncertainties in Single-Sample Experiments," *ASME* Mechanical Engineering, Vol. 75, pp. 3-8. (1953)
17. Kartens, C.W., "Effects of Air Entrainment on the Damping Coefficients of a Squeeze Film Damper," Senior Honor Thesis, Texas A&M University, (1997).
18. Beets, T.A., Díaz, S. E. and San Andrés, L.A., "Pressure Measurement and Flow Visualization on a SFD With a Bubbly Lubricant," Proceedings of the 2000 NSF Design & Manufacturing Research Conference, Vancouver, Canada, January 3-6, (2000).

Appendix 1
Parameters derived from sine-sweep load experiments

Appendix 2
System flexibilities for tests with sine sweep loads

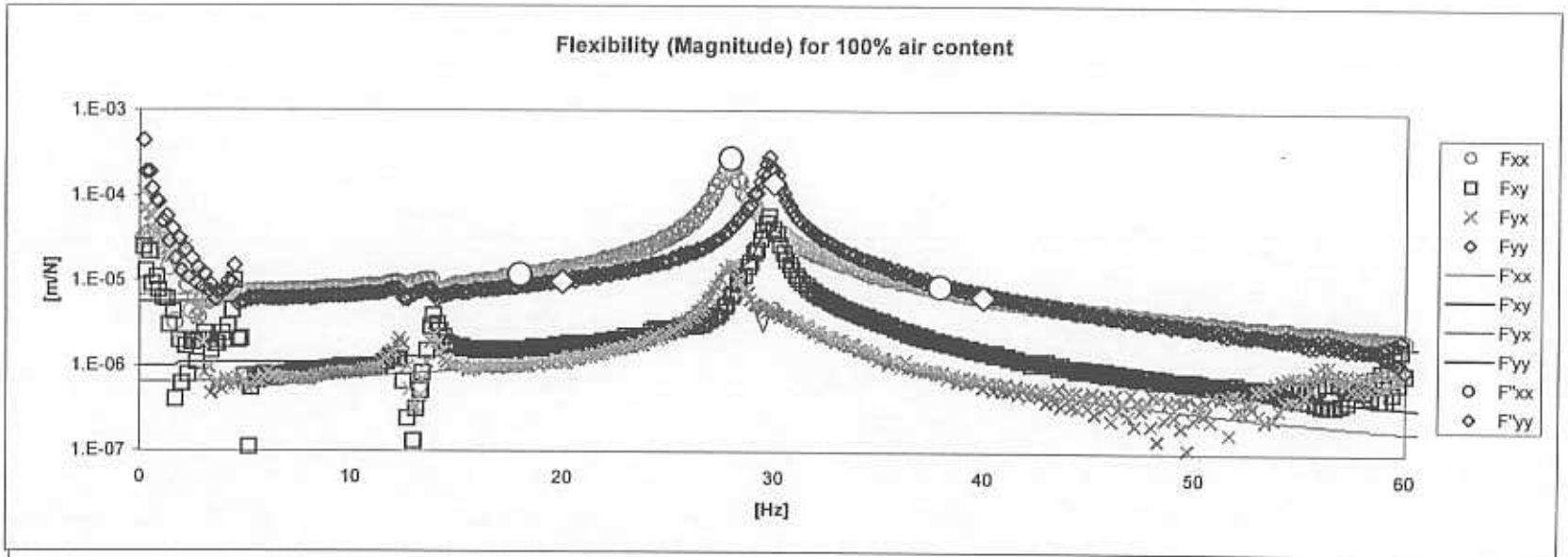
Flexibility (Magnitude) for 100% air content
1.E-03
1.E-04
1.E-05
1.E-06
1.E-07
[m/N]
0
10
20
30
40
50
60
[Hz]
Fxx
Fxy
Fyx
Fyy
F'xx
F'xy
F'yx
F'yy
F'xx
F'yy

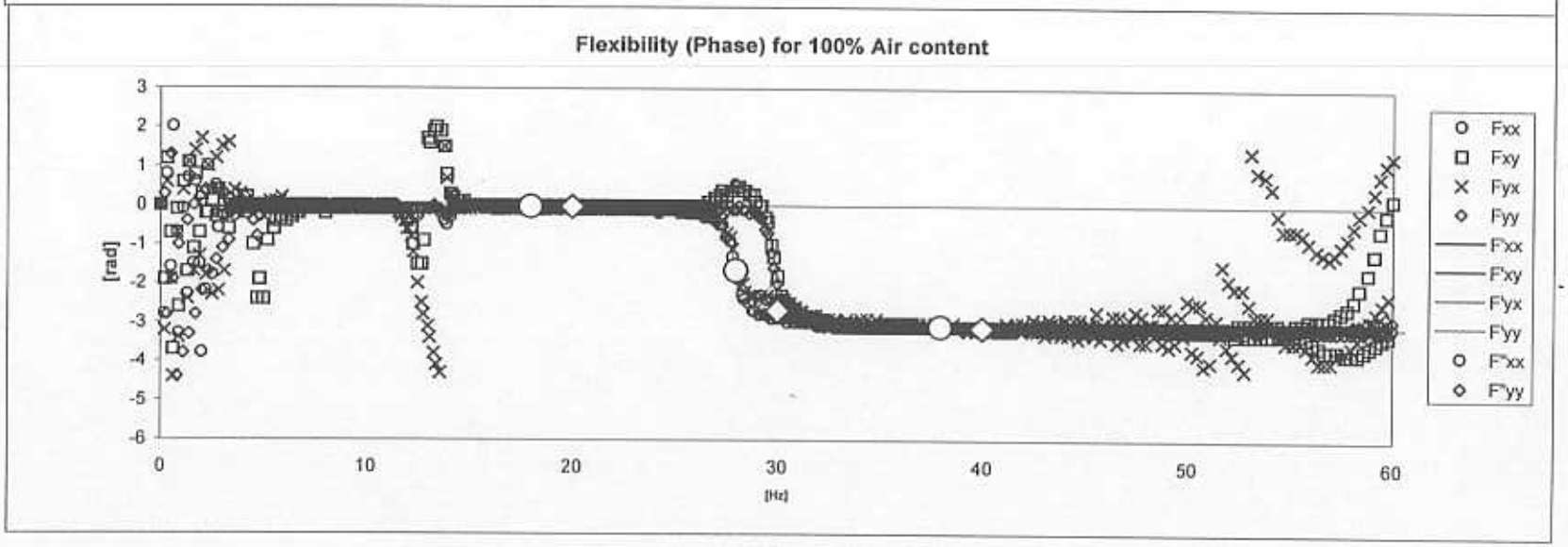
Flexibility (Phase) for 100% Air content
3
2
1
0
-1
-2
-3
-4
-5
-6
[rad]
0
10
20
30
40
50
60
[Hz]
Fxx
Fxy
Fyx
Fyy
F'xx
F'xy
F'yx
F'yy
F'xx
F'yy

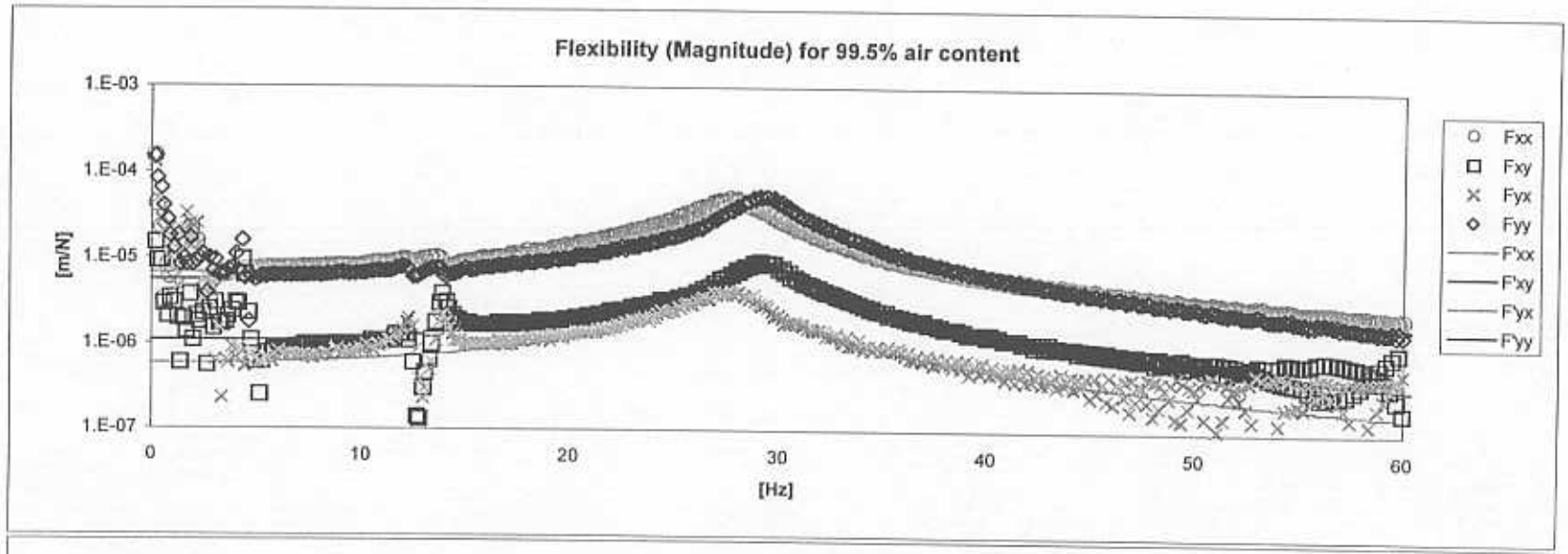
Flexibility (Magnitude) for 99.5% air content
1.E-03
1.E-04
1.E-05
1.E-06
1.E-07
[m/N]
0
10
20
30
40
50
60
[Hz]
Fxx
Fxy
Fyx
Fyy
F'xx
F'xy
F'yx
F'yy

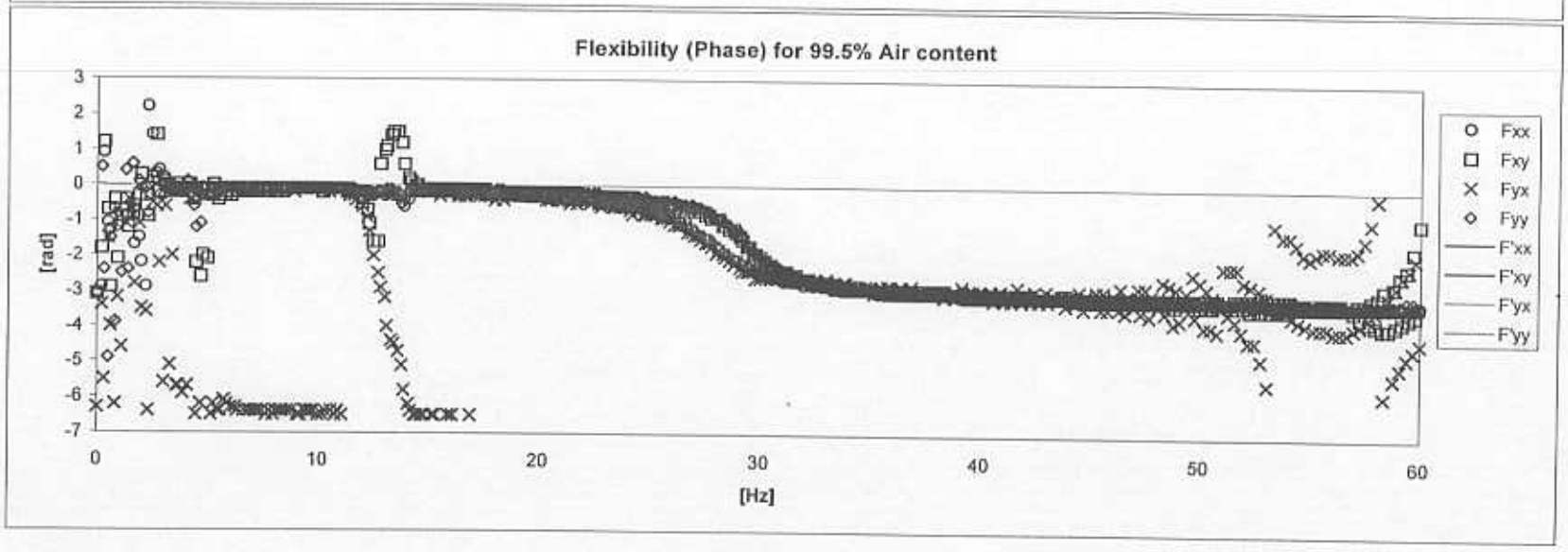
Flexibility (Phase) for 99.5% Air content
3
2
1
0
-1
-2
-3
-4
-5
-6
-7
[rad]
0
10
20
30
40
50
60
[Hz]
Fxx
Fxy
Fyx
Fyy
F'xx
F'xy
F'yx
F'yy

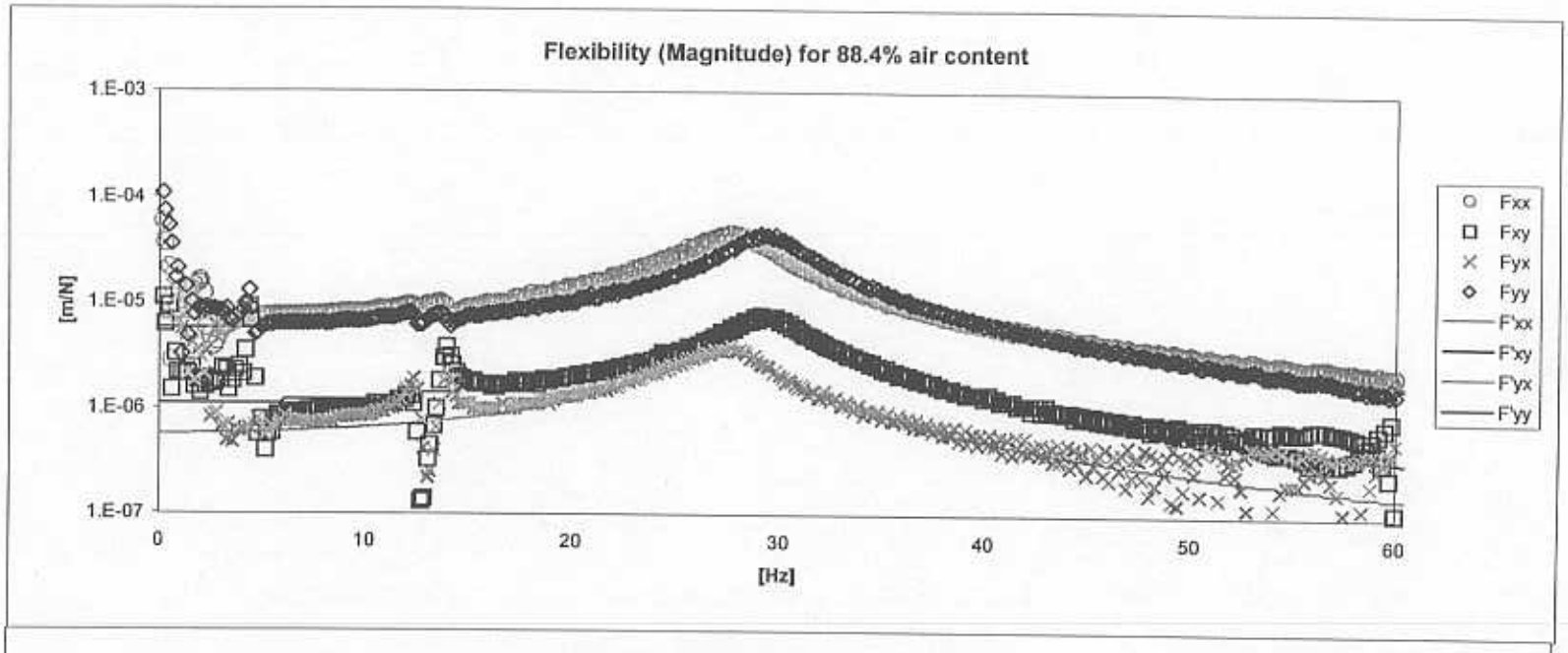
Flexibility (Magnitude) for 88.4% air content
1.E-03
1.E-04
1.E-05
1.E-06
1.E-07
[m/N]
0
10
20
30
40
50
60
[Hz]
Fxx
Fxy
Fyx
Fyy
F'xx
F'xy
F'yx
F'yy

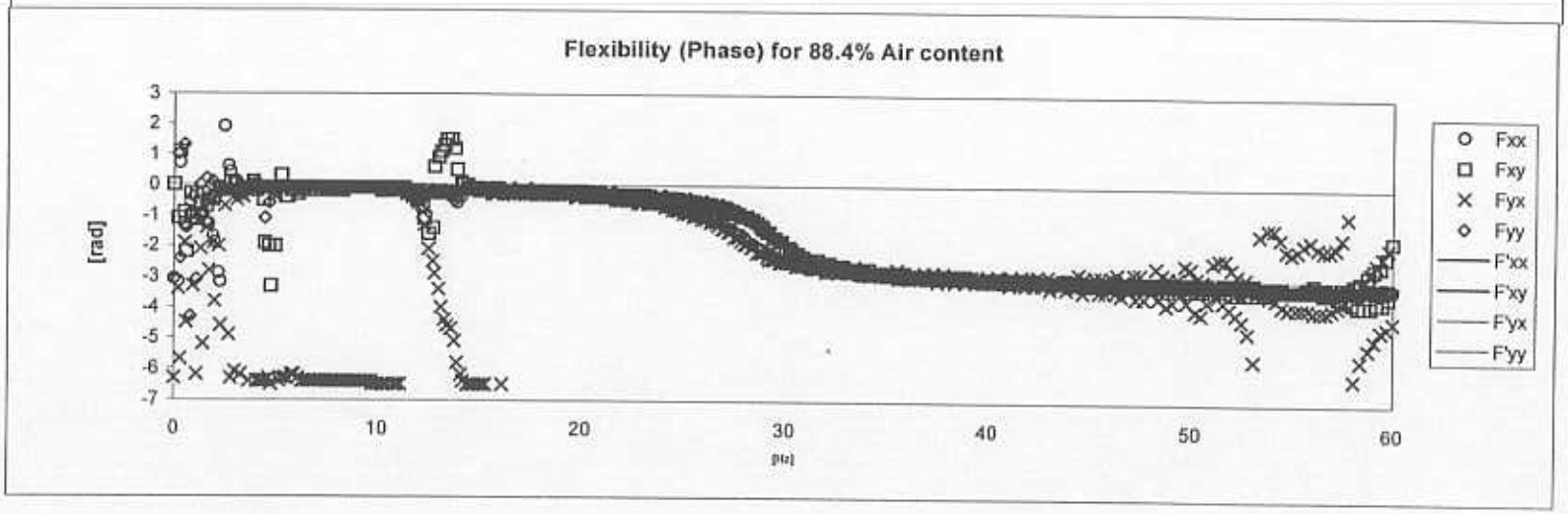
Flexibility (Phase) for 88.4% Air content
3
2
1
0
-1
-2
-3
-4
-5
-6
-7
[rad]
0
10
20
30
40
50
60
[Hz]
Fxx
Fxy
Fyx
Fyy
F'xx
F'xy
F'yx
F'yy

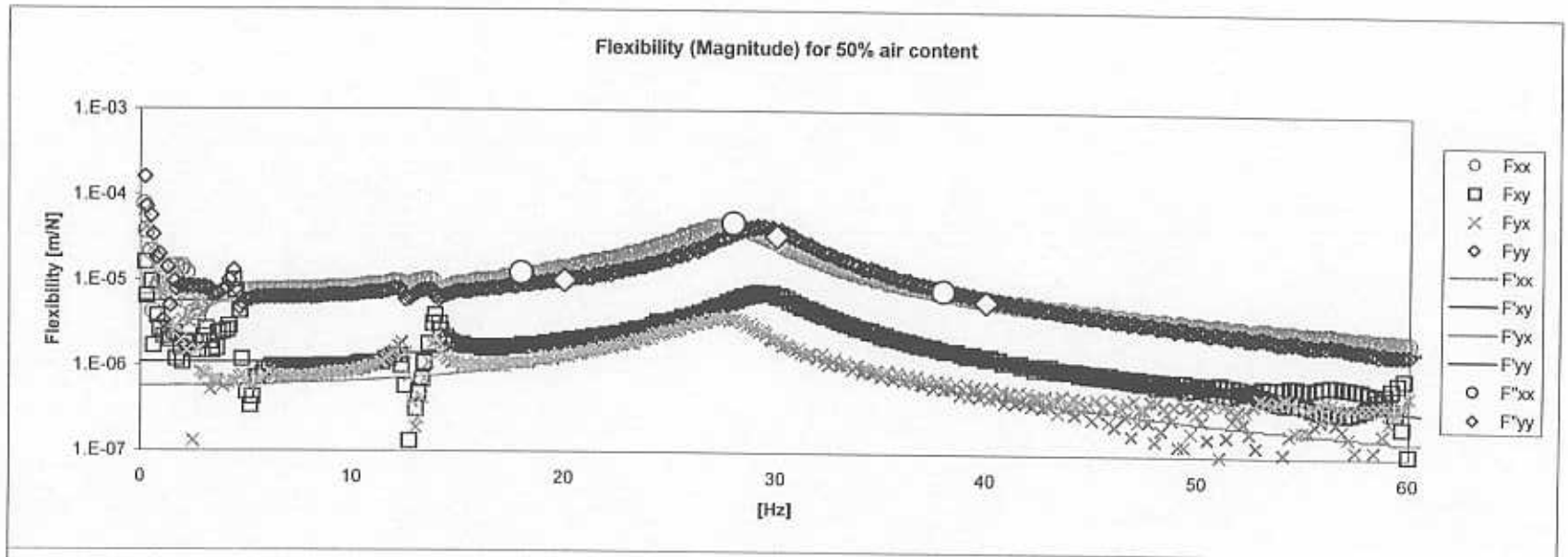
Flexibility (Magnitude) for 50% air content
Flexibility [m/N]
1.E-03
1.E-04
1.E-05
1.E-06
1.E-07
0
10
20
30
40
50
60
[Hz]
Fxx
Fxy
Fyx
Fyy
F'xx
F'xy
F'yx
F'yy
F"xx
F"yy

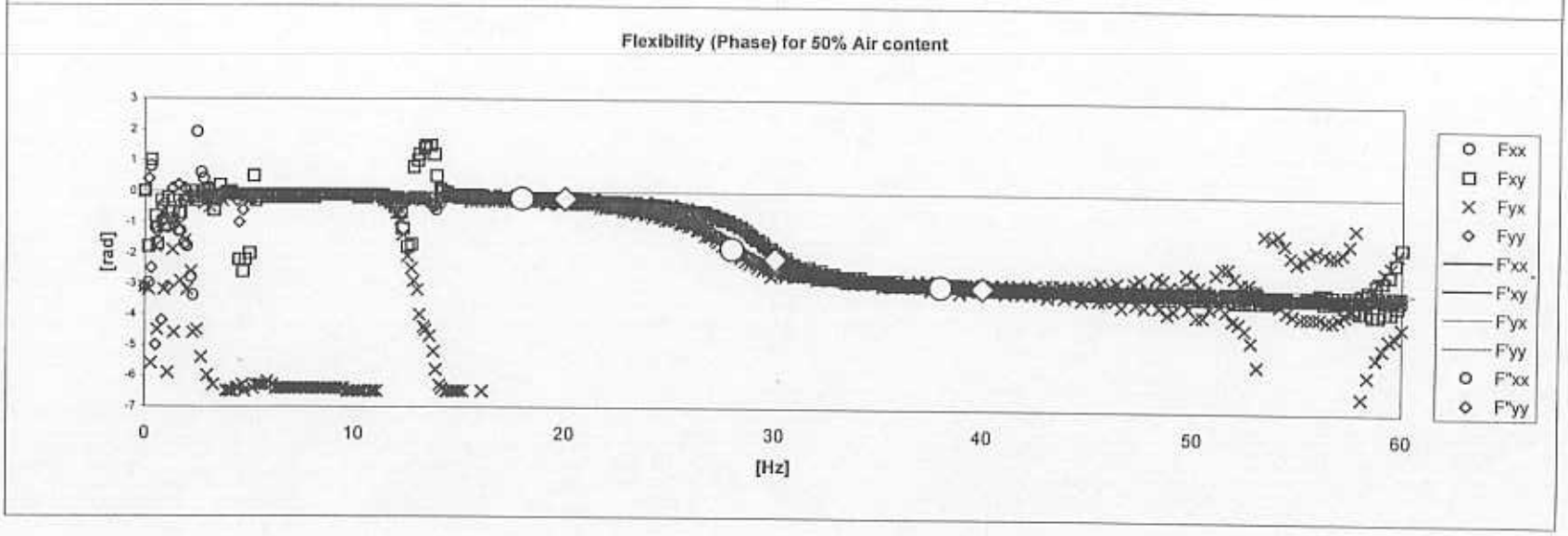
Flexibility (Phase) for 50% Air content
[rad]
3
2
1
0
-1
-2
-3
-4
-5
-6
-7
0
10
20
30
40
50
60
[Hz]
Fxx
Fxy
Fyx
Fyy
F'xx
F'xy
F'yx
F'yy
F"xx
F"yy

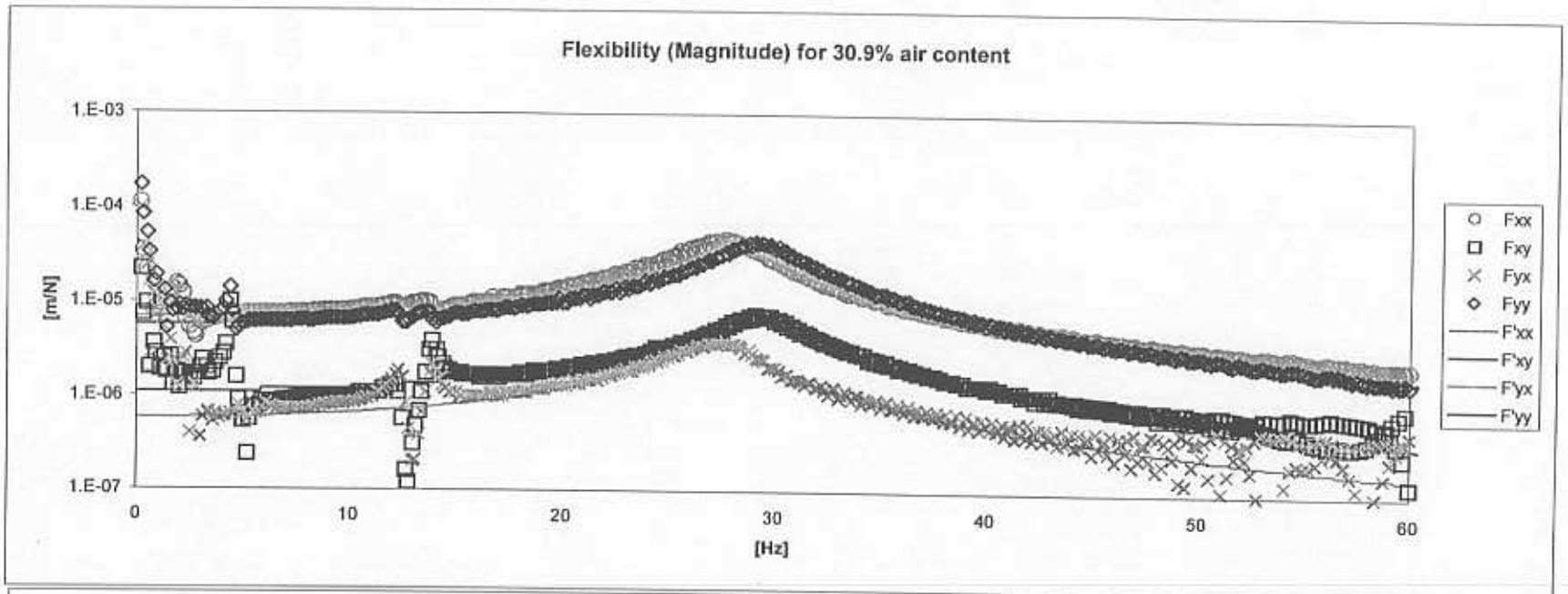
Flexibility (Magnitude) for 30.9% air content
1.E-03
1.E-04
1.E-05
1.E-06
1.E-07
[m/N]
0
10
20
30
40
50
60
[Hz]
Fxx
Fxy
Fyx
Fyy
F'xx
F'xy
F'yx
F'yy

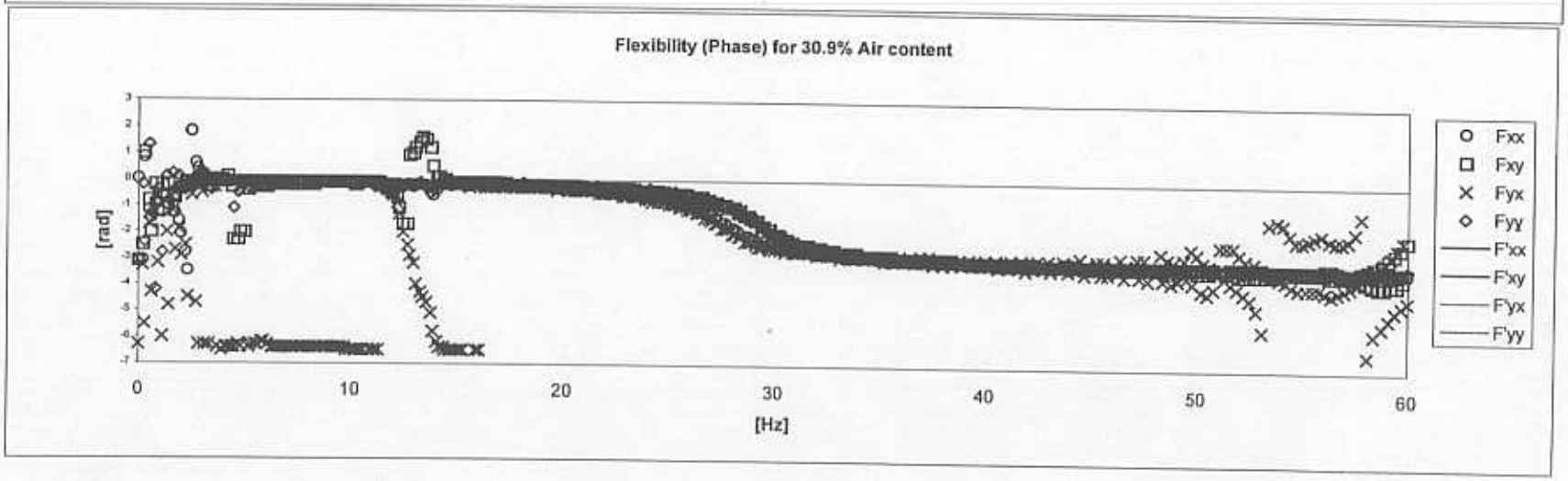
Flexibility (Phase) for 30.9% Air content
[rad]
0
10
20
30
40
50
60
[Hz]
Fxx
Fxy
Fyx
Fyy
F'xx
F'xy
F'yx
F'yy

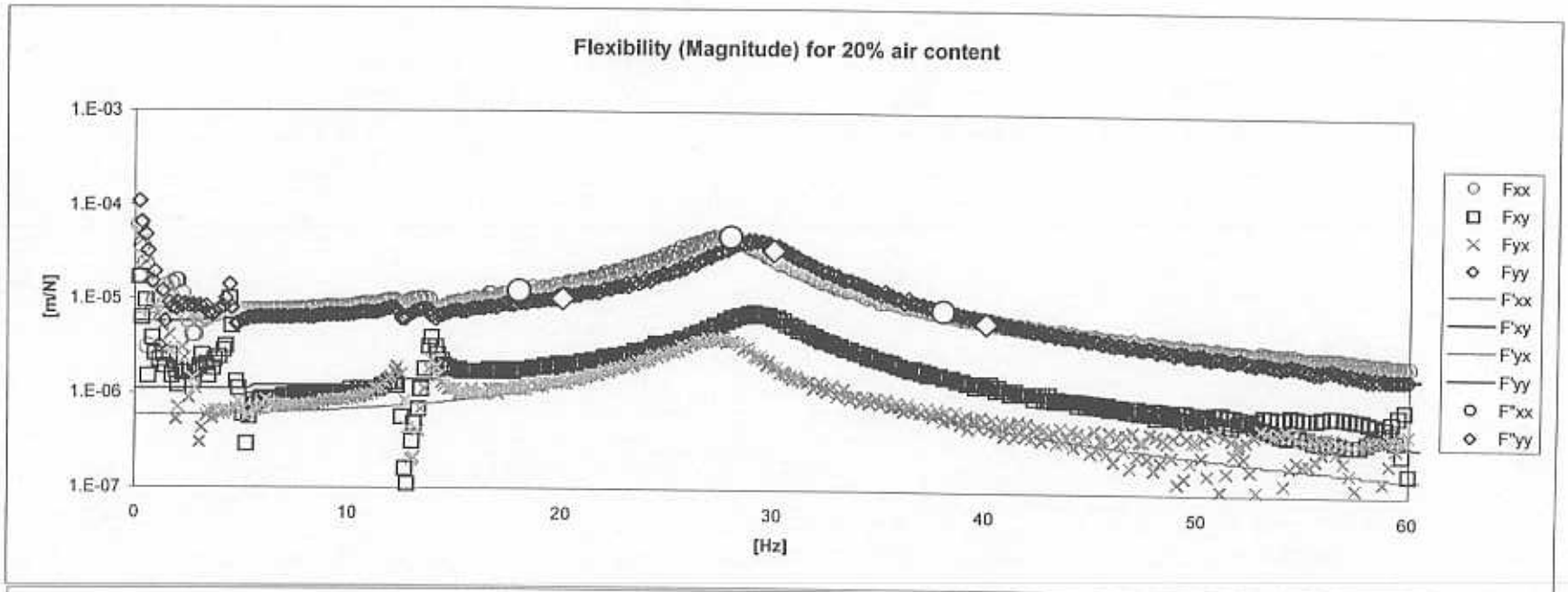
Flexibility (Magnitude) for 20% air content
1.E-03
1.E-04
1.E-05
1.E-06
1.E-07
[m/N]
0
10
20
30
40
50
60
[Hz]
Fxx
Fxy
Fyx
Fyy
F'xx
F'xy
F'yx
F'yy
F"xx
F"yy

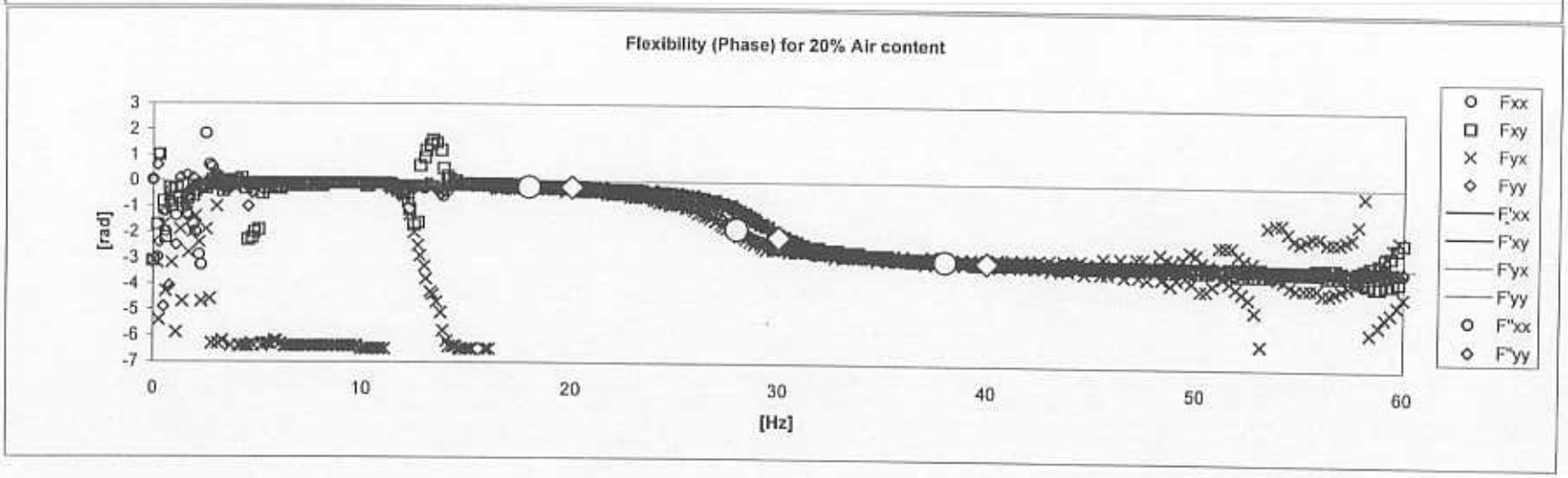
Flexibility (Phase) for 20% Air content
3
2
1
0
-1
-2
-3
-4
-5
-6
-7
[rad]
0
10
20
30
40
50
60
[Hz]
Fxx
Fxy
Fyx
Fyy
F'xx
F'xy
F'yx
F'yy
F"xx
F"yy

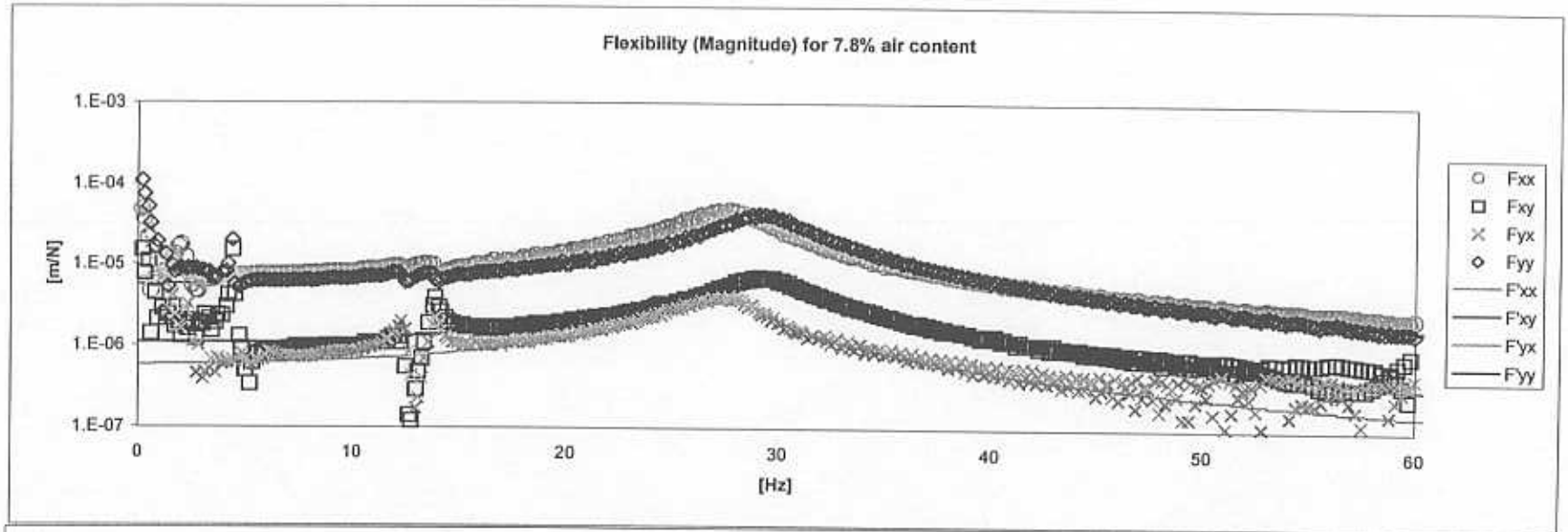
Flexibility (Magnitude) for 7.8% air content
1.E-03
1.E-04
1.E-05
1.E-06
1.E-07
[m/N]
0
10
20
30
40
50
60
[Hz]
Fxx
Fxy
Fyx
Fyy
F'xx
F'xy
F'yx
F'yy

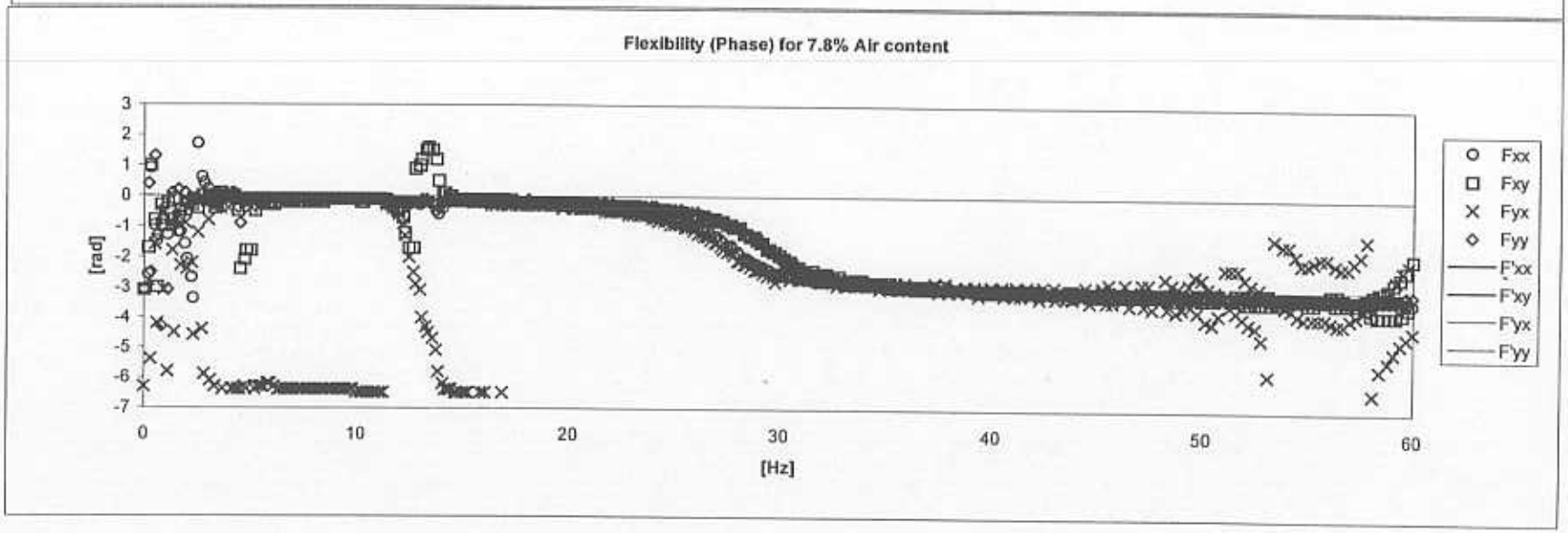
Flexibility (Phase) for 7.8% Air content
3
2
1
0
-1
-2
-3
-4
-5
-6
-7
[rad]
0
10
20
30
40
50
60
[Hz]
Fxx
Fxy
Fyx
Fyy
F'xx
F'xy
F'yx
F'yy

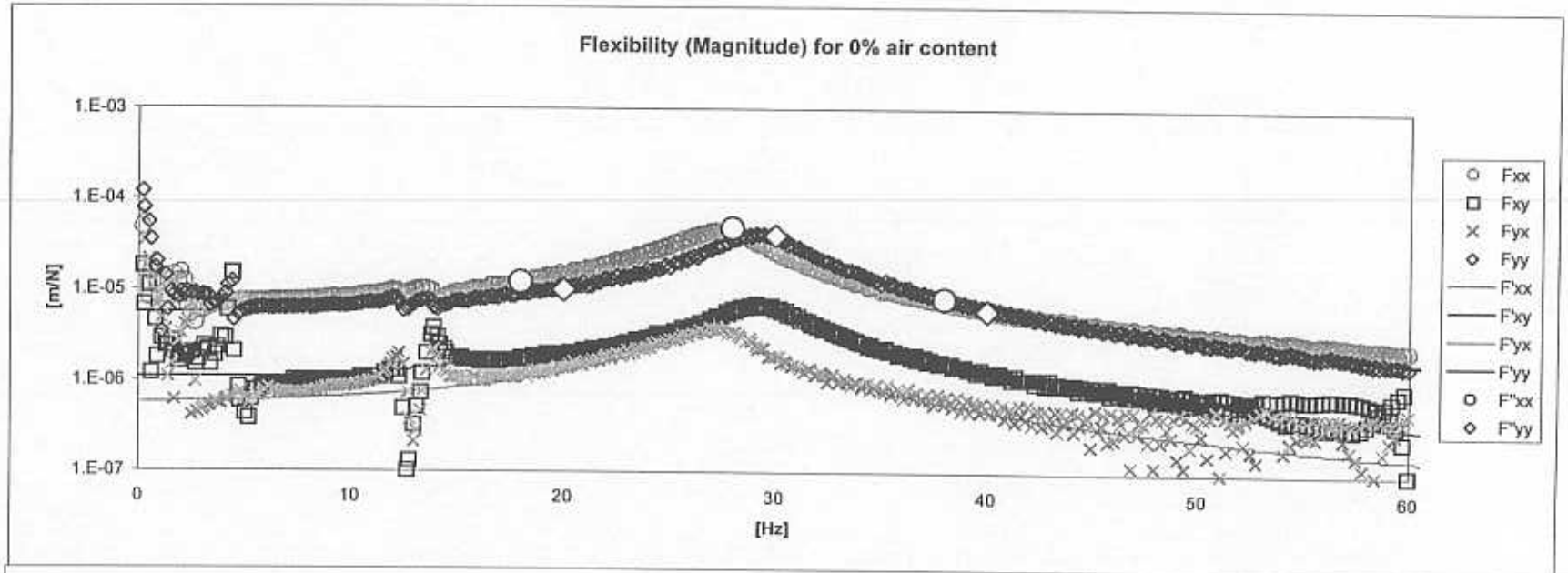
Flexibility (Magnitude) for 0% air content
1.E-03
1.E-04
1.E-05
1.E-06
1.E-07
[m/N]
0
10
20
30
40
50
60
[Hz]
Fxx
Fxy
Fyx
Fyy
F'xx
F'xy
F'yx
F'yy
F"xx
F"yy

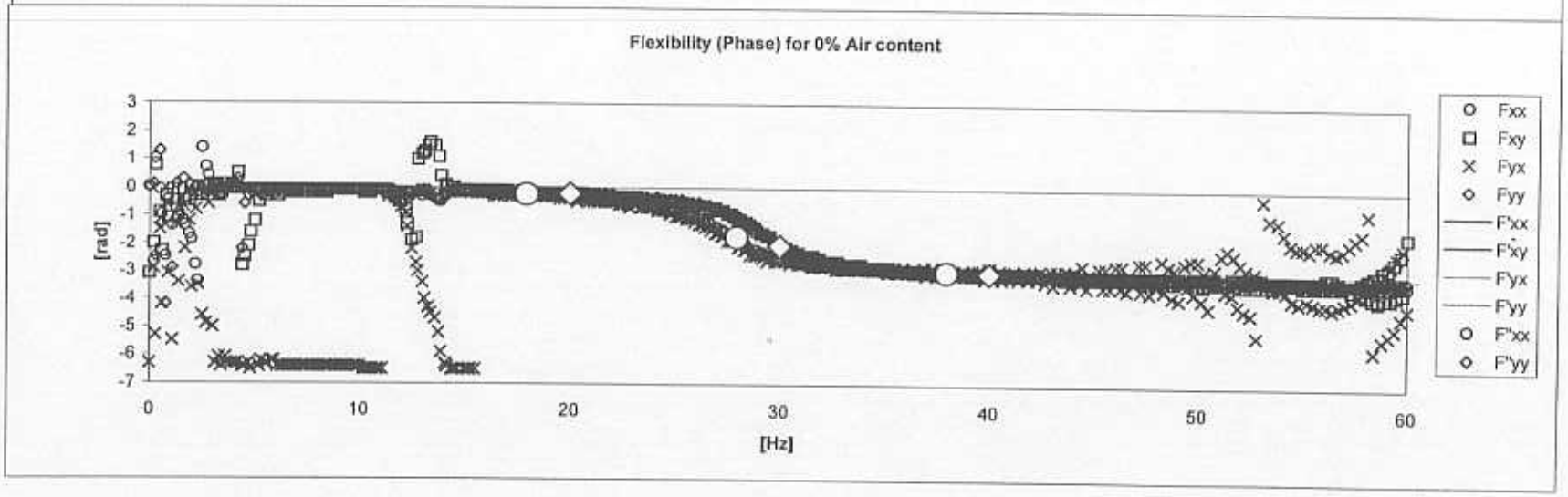
Flexibility (Phase) for 0% Air content
3
2
1
0
-1
-2
-3
-4
-5
-6
-7
[rad]
0
10
20
30
40
50
60
[Hz]
Fxx
Fxy
Fyx
Fyy
F'xx
F'xy
F'yx
F'yy
F"xx
F"yy

Appendix 3
Results of single frequency experiments

Harmonic Excitation Tests

In these tests, as in the sine sweep load experiments, the rotor is excited with a harmonic force applied by the shakers at the *SFD* location. Three different frequencies are used to excite the rotor in each direction of motion.. Within the frequency range tested, the rotor vibrates in a conical mode of vibration with the pivot at the bushing, so the system has only two uncoupled degrees of freedom *(X,Y)*.

A least squares approximation of the real and imaginary parts of the measured impedances at three different frequencies is used to identify the dynamic parameters. The equation of motion in the *X* direction is expressed as

$$m\ddot{x}_i(t) + c\dot{x}_i(t) + kx_i(t) = f_i(t) \tag{3.1}$$

where i=1,3. Applying the FFT to equation 1 leads to

$$-\omega_i^{\,2} mX(\omega_i) + i\omega_i cX(\omega_i) + kX(\omega_i) = F(\omega_i) \tag{3.2}$$

and expressed in matrix form as

$$\begin{bmatrix} -\omega_1^2 & i\omega_1 & 1 \\ -\omega_2^2 & i\omega_2 & 1 \\ -\omega_3^2 & i\omega_3 & 1 \end{bmatrix} \cdot \begin{bmatrix} m \\ c \\ k \end{bmatrix} = \begin{bmatrix} \dfrac{F(\omega_1)}{X(\omega_1)} \\ \dfrac{F(\omega_2)}{X(\omega_2)} \\ \dfrac{F(\omega_3)}{X(\omega_3)} \end{bmatrix} = \begin{bmatrix} H_1(\omega_1) \\ H_2(\omega_2) \\ H_3(\omega_3) \end{bmatrix} \tag{3.3}$$

Separating equation (3.3) into its real and imaginary parts gives

$$\begin{bmatrix} -\omega_1^2 & 0 & 1 \\ 0 & 1 & 0 \\ -\omega_2^2 & 0 & 1 \\ 0 & 1 & 0 \\ -\omega_3^2 & 0 & 1 \\ 0 & 1 & 0 \end{bmatrix} \cdot \begin{bmatrix} m \\ c \\ k \end{bmatrix} = \begin{bmatrix} \mathrm{Re}(H_1) \\ \mathrm{Im}(H_1)/\omega_1 \\ \mathrm{Re}(H_2) \\ \mathrm{Im}(H_2)/\omega_2 \\ \mathrm{Re}(H_3) \\ \mathrm{Im}(H_3)/\omega_3 \end{bmatrix} \tag{3.4}$$

Thus, the least-square solution for the parameters *(m, c, k)* is

$$\begin{bmatrix} m \\ c \\ k \end{bmatrix} = (A^T A)^{-1} A^T \begin{bmatrix} \mathrm{Re}(H_1) \\ \mathrm{Im}(H_1)/\omega_1 \\ \mathrm{Re}(H_2) \\ \mathrm{Im}(H_2)/\omega_2 \\ \mathrm{Re}(H_3) \\ \mathrm{Im}(H_3)/\omega_3 \end{bmatrix} \tag{3.5}$$

$$\text{Where } A = \begin{bmatrix} -\omega_1^2 & 0 & 1 \\ 0 & 1 & 0 \\ -\omega_2^2 & 0 & 1 \\ 0 & 1 & 0 \\ -\omega_3^2 & 0 & 1 \\ 0 & 1 & 0 \end{bmatrix}. \tag{3.6}$$

A similar analysis is conducted for motions in the vertical direction. Note that cross-coupled effects have altogether been neglected presently. The excitation frequencies chosen were

	Vertical	Horizontal
ω_1 [Hz]	20	18
ω_2 [Hz]	30 (Natural)	28 (Natural)
ω_3 [Hz]	40	38

Table 3.1 show the identified direct inertia (M), stiffness (K) and damping (C) coefficients derived from the harmonic excitation tests. These coefficients correlate well with those derived from the sine sweep load tests.

Table 3.1 Force coefficients determined from single frequency experiments

λ volume fraction	$\delta\lambda$	M_{xx} [kg]	M_{yy} [kg]	K_{xx} [KN/m]	K_{yy} [kN/m]	C_{xx} [Ns/m]	C_{yy} [Ns/m]
0	0	4.57	5.50	138.16	184.53	124.73	122.95
0.5770	0.1408	4.57	5.48	137.95	184.11	124.65	123.68
0.5038	0.0727	4.60	5.49	137.62	181.73	116.57	122.89
0.2107	0.0593	4.59	5.48	136.74	180.60	117.17	123.74
1	0	4.51	5.32	141.10	184.45	24.35	12.03
AVERAGE	-	4.57	5.45	138.31	183.09		
Uncertainty	-	0.10	0.23	4.95	5.42		